Quantum-chromodynamic approach for the large-transverse-momentum production of particles and jets

R. P. Feynman, R. D. Field, and G. C. Fox

California Institute of Technology, Pasadena, California 91125

(Received 15 May 1978)

It is shown that if, in a calculation of high-transverse-momentum ($p_\perp$) meson production in hadron-hadron collisions, one includes not only the scale-breaking effects that might be expected from asymptotically free theories but also the effects due to the transverse momentum of quarks in hadrons *and* further adds contributions from quark-gluon and gluon-gluon scattering to those of quark-quark scattering *then* the results are not inconsistent with the data. The approach yields the correct magnitude and an apparent approximate $1/p_\perp^8$ behavior in accord with single-particle data for the energy range currently observed. Two-particle correlations are examined. Because of scale-breaking effects and the presence of gluons, the theory does not have the problem of predicting too many away-side hadrons at large $p_\perp$ as did an earlier quark-quark scattering "black-box" approach. We conclude that the quantum-chromodynamics approach is in reasonable accord with the data although theoretical uncertainties (especially at low $p_\perp$) make incontrovertible conclusions impossible at present. Crucial tests of the theory require higher $p_\perp$ than are now available; estimates for this region are made.

I. INTRODUCTION

We investigate whether the present experimental behavior of mesons with large transverse momentum in hadron-hadron collisions is consistent with the theory of quantum-chromodynamics (QCD) with asymptotic freedom, at least as the theory is now partially understood. It is shown that if things behave more or less according to current theoretical ideas, the experimental data at high $p_\perp$ would be explicable with reasonable choices for currently unknown quantities (such as the distribution of gluons in the proton and the fragmentation functions describing gluon jets). The theory of QCD might provide an adequate explanation of all the experimental results that we have discussed in previous papers (hereafter referred to as FF1[1] and FFF[2]).

We and others[3-9] investigated this large-$p_\perp$ experimental behavior phenomenologically. In particular, the view that large-$p_\perp$ mesons are generated by hard large-angle collisions between quarks present in the initial hadrons has been found to be very fruitful. The outgoing quarks are assumed not to come out freely, but to distribute their momentum over a series of hadrons that form a "jet" in the general direction of the "original quark."

This view when compared in detail with all available experiments is found to be successful in many regards. In particular, the distributions of particles in single-arm experiments and the large ratio of jet to particle cross sections are successfully interpreted or predicted. To do this, the differential cross section for quark-quark collisions, $d\hat{\sigma}/d\hat{t}$ ("black-box" cross sections),

was taken to vary as $f(\hat{t}/\hat{s})\hat{s}^{-4}$ in disagreement with field theory which expects $\hat{s}^{-2}$ behavior. The size and angular dependence, 2300 mb/$(-\hat{s}\hat{t}^3)$, was chosen empirically. In addition, in FF1 and FFF, the effects of collisions of gluons (as constituents within hadrons) were omitted. At that time, there was no experimental evidence to require their existence.

The $f(\hat{t}/\hat{s})\hat{s}^{-4}$ behavior was chosen as a direct result of assumptions that parton distributions scaled with energy and the observation that experiments done at two or more different center-of-mass energies W but at a fixed $x_\perp = 2p_\perp/W$ and fixed angle showed the invariant cross section varying as $p_\perp^{-8}$.

It is necessary to include a transverse momentum, $(k_\perp)_{h \to q}$, of the quarks within the initial hadrons to account for much of the data[2,10-14]; for example, observations in two-arm experiments of P_{out} (Ref. 15) (i.e., lack of coplanarity of the beam, target, and two outgoing hadrons).[16] Some of the apparent large $p_\perp$ of a hadron can be due to the initial transverse momentum of the incoming quarks. This vitiates the direct scaling connection between a $d\hat{\sigma}/d\hat{t} = f(\hat{t}/\hat{s})\hat{s}^{-n}$ and the invariant cross section behaving like $p_\perp^{-2n}$ at fixed $x_\perp$ and $\theta_{c.m.}$. However, as long as $\langle k_\perp \rangle_{h \to q}$ is 500 MeV or less, the effects on the single-particle invariant cross section are not great and in FFF we limited ourselves to values not higher than this.

There are, however, two serious discrepancies with experiment which indicate that, in spite of the successes, something is wrong with the black-box model. First, recently measured values of P_{out} seem to be higher than expected so that $\langle k_\perp \rangle_{h \to q}$ must exceed 500 MeV. That would mean

that the scaling argument leading to $\hat{s}^{-4}$ for the quark-quark cross section was wrong in the range of data used. That is, the $p_\perp^{-8}$ behavior of experiment would be *accidental* and not fundamental. For example, a quark-quark cross section varying only as $\hat{s}^{-3}$ could (with a $\langle k_\perp \rangle_{h \to q}$ big enough to explain the large P_{out}'s observed) produce an apparent $p_\perp^{-8}$ hadron scaling.

Second, in two-arm experiments with events triggered on one side by a high-$p_\perp$ hadron (the "toward" side), the number of particles with large $p_\perp$ on the opposite side (the "away" side) was experimentally only about $\frac{1}{3}$ of the number predicted. Some of this is accounted for by increasing $\langle k_\perp \rangle_{h \to q}$, but not all, by far. The only explanation available in the approach is that the outgoing momentum on the away side is distributed more softly (distributed among more hadrons of lower momentum) than is typical of a quark; that is, there is more than one component contributing to the high-transverse-momentum jets. This is evidence for the need to include gluons as well as quarks in the description of high-$p_\perp$ phenomena. It requires both gluons and the assumption that gluons fragment into a distribution of hadrons of lower average momentum than does a quark.

These discrepancies lead us to include gluons in an analysis of high-$p_\perp$ hadron-hadron collisions, and to the further suggestion that QCD field theory might not be inconsistent with what is observed. Although with large values of $\langle k_\perp \rangle_{h \to q}$, the scattering cross section behaving like $f(\hat{t}/\hat{s})\hat{s}^{-3}$ will yield a $p_\perp^{-8}$ behavior over the range of data, this still differs from the naive field-theory expectation of $\hat{s}^{-2}$. (Including gluons does not help produce a $p_\perp^{-8}$ behavior.) But in the theory of QCD, there are a number of small scale-breaking effects to notice. The effective coupling constant falls logarithmically with energy. The incoming parton distributions should not scale, but at high x should fall and at small x rise as Q^2 increases. Effects in this direction are already seen in ep and μp scattering and have been analyzed in Refs. 17–20. An analogous modification of the fragmentation functions $D_q^h(z)$ is also expected theoretically. None of these effects alone change the effective apparent $p_\perp$ power index N_{eff} in $p_\perp^{-N_{eff}}$ very much and yet they all work in the same direction and together, as we show, they can change N_{eff} from the naive 4 to about 6 in the energy range of present experiments. (The scale breaking due to the large value of $\langle k_\perp \rangle_{h \to q}$ then brings N_{eff} to about 8 over this range.)

Thus the possibility exists that QCD can provide the full explanation of all the high-energy high-$p_\perp$ experimental results. We analyze this possibility in this paper. Some of our findings have been

presented in Refs. 21 and 22. We wish to explain our approach in detail here. The net result is to demonstrate that this possibility is very real.[23]

The main problem in such an analysis is that no complete calculation of a prediction for QCD for any phenomenon—even qualitative ones such as the confinement of quarks—has yet been made. At present, the mathematical complexities are still too great. However, at very high energy or high momentum transfer Q, the theory is asymptotically free; the effective coupling constant falls with increasing Q^2. As emphasized by Politzer,[26] this permits calculation of those parts of a collision involving high Q^2. Yet every real process involves high and low Q^2 together and the precise separation of these parts and hence exact definition of the theory for hadron-hadron collisions is a problem for the (we hope near) future. We shall proceed here in a preliminary way.

What we do is include all the ingredients thought to be present from existing ideas on QCD. We assume that the effective coupling behaves as $\alpha_s(Q^2) = 12\pi/(25 \ln Q^2/\Lambda^2)$ with Λ determined from the scale breaking observed in ep and μp collisions. The distribution of constituents i (quarks and gluons) in the proton $G_{p \to i}(x, Q^2)$ and their fragmentation functions $D_i^h(z, Q^2)$ are given a Q^2 dependence in accord with QCD analyses of ep and μp collisions. The theory gives formulas for scaling violations (Q^2 dependences), but the functions must be known at some nominal reference momenta, say Q_0^2. The distributions $G_{p \to i}(x, Q_0^2)$ are determined from fits to the ep and μp data. For the quark fragmentation functions $D(z, Q_0^2)$ we use the distributions of our previous quark-jet paper[27] and take $Q_0^2 = 4$ GeV^2. We hope that data on the quark fragmentation functions from e^+e^-, ep, μp, or νp experiments will soon be available to test the Q^2 dependence expected from QCD and to allow for a more precise determination of them.

For the fundamental constituent cross sections for quark-quark, quark-gluon, and gluon-gluon scattering, we have taken the first-order perturbation scattering expected from QCD[28,29] (see Table I) and normalized absolutely by the effective coupling $\alpha_s(Q^2)$. This replaces the arbitrary size, energy dependence, and angular dependence of the black box in our previous papers.

Thus it would seem that we have little freedom of arbitrary choice. This would be true were it not for the distributions of gluons in the proton $G_{h \to g}(x, Q_0^2)$, and the distribution of hadrons in a gluon jet $D_g^h(z, Q_0^2)$, at the reference momenta. These two functions are not constrained much by other experiments and are thus essentially arbitrary. We have chosen these with an eye to experiment. In particular, we have chosen $D_g^h(z, Q_0^2)$

TABLE I. Cross sections for the various constituent quark-quark, quark-gluon, and gluon-gluon subprocesses.[a] The differential cross section is given by $d\hat{\sigma}/d\hat{t} = \pi\alpha_s^2(Q^2)|A|^2/\hat{s}^2$, where $\alpha_s(Q^2)$ is the effective coupling given by Eq. (3.1).

	Subprocess	$|A|^2$
1.	$q_iq_j \rightarrow q_iq_j$ $q_i\bar{q}_j \rightarrow q_i\bar{q}_j$ $(i \neq j)$	$\dfrac{4}{9}\dfrac{\hat{s}^2+\hat{u}^2}{\hat{t}^2}$
2.	$q_iq_i \rightarrow q_iq_i$	$\dfrac{4}{9}\left(\dfrac{\hat{s}^2+\hat{u}^2}{\hat{t}^2}+\dfrac{\hat{s}^2+\hat{t}^2}{\hat{u}^2}\right)-\dfrac{8}{27}\dfrac{\hat{s}^2}{\hat{u}\hat{t}}$
3.	$q_i\bar{q}_i \rightarrow q_i\bar{q}_i$	$\dfrac{4}{9}\left(\dfrac{\hat{s}^2+\hat{u}^2}{\hat{t}^2}+\dfrac{\hat{t}^2+\hat{u}^2}{\hat{s}^2}\right)-\dfrac{8}{27}\dfrac{\hat{u}^2}{\hat{s}\hat{t}}$
4.	$q_i\bar{q}_i \rightarrow gg$	$\dfrac{32}{27}\left(\dfrac{\hat{u}^2+\hat{t}^2}{\hat{u}\hat{t}}\right)-\dfrac{8}{3}\left(\dfrac{\hat{u}^2+\hat{t}^2}{\hat{s}^2}\right)$
5.	$gg \rightarrow q_i\bar{q}_i$	$\dfrac{1}{6}\left(\dfrac{\hat{u}^2+\hat{t}^2}{\hat{u}\hat{t}}\right)-\dfrac{3}{8}\left(\dfrac{\hat{u}^2+\hat{t}^2}{\hat{s}^2}\right)$
6.	$q_ig \rightarrow q_ig$	$-\dfrac{4}{9}\left(\dfrac{\hat{u}^2+\hat{s}^2}{\hat{u}\hat{s}}\right)+\left(\dfrac{\hat{u}^2+\hat{s}^2}{\hat{t}^2}\right)$
7.	$gg \rightarrow gg$	$\dfrac{9}{2}\left(3-\dfrac{\hat{u}\hat{t}}{\hat{s}^2}-\dfrac{\hat{u}\hat{s}}{\hat{t}^2}-\dfrac{\hat{s}\hat{t}}{\hat{u}^2}\right)$

[a] This table is identical to that in Ref. 29.

"softer" than $D_q^h(z, Q_0^2)$ because of experimental features of high-$p_\perp$ processes, and our success depends on this choice in several of the comparisons.

The theory of QCD also may explain how P_{out} can be so large.[26,30-33] For example, sometimes two quarks hit and scatter to two quarks plus a relatively hard radiated gluon, so that the two outgoing quark jets are out of momentum coplanarity by the momentum of the gluon. These effects can be calculated, and we are engaged in such calculations. What we have done here is a temporary expedient. We have simply taken the $k_\perp$ distribution measured for $\mu^+\mu^-$ pairs in pp collisions (where similar gluon emissions are possible) as a measure of an "effective" $k_\perp$ of quarks in the initial hadrons to mimic the effect of such $2 \rightarrow 3$ constituent processes. This is not precisely correct and the Q^2 and x dependence of the high-$k_\perp$ tail to the effective transverse momentum of quarks in the hadrons is not handled properly in this manner. We hope to improve on this at a later date.

We begin in Sec. II by reviewing the successes of the quark-quark black-box approach and to examine closely its failures. The ingredients used in our QCD approach to high-$p_\perp$ processes are explained in Sec. III and the results presented in Sec. IV. We reserve Sec. V for summary and conclusions. The agreement with experiment is

very satisfactory. Quantum chromodynamics might well be the correct theory behind these phenomena.

II. THE QUARK-QUARK SCATTERING BLACK-BOX APPROACH[1-10]

A. Successes

In spite of the rather *ad hoc* way in which we adjusted the quark-quark scattering cross section $d\hat{\sigma}/d\hat{t}$, many predictions of the black-box approach did not depend sensitively on it and were in agreement with experiment. As discussed in the summary of FFF, the conclusions that did not depend strongly on the precise value of the internal transverse momenta of the quarks with hadrons were the most successful. They include:

(1) Predictions for the large-$p_\perp$ single-particle ratios were quite successful. The π^+/π^- (and K^+/K^-) ratios were predicted to become larger at high $x_\perp$ since in this region the constituents that collide are predominantly u quarks that fragment more often into π^+ (K^+) than π^- (K^-). Similarly, the mixing of the η meson implied that η/π^0 should be about $\frac{1}{2}$ at high $x_\perp$ also in agreement with data. The high-$x_\perp$ K^+/π^+ ratio was used to deduce that $D_u^{K^+}(z)/D_u^{\pi^+}(z)$ must be about $\frac{1}{2}$ at large z. Recent lepton data are consistent with this deduction.[34]

(2) The number of π^0's[35] and jets[36-38] produced with a pion or proton beam is consistent with the expectation that the quarks in a pion carry, on the average, more momentum than they do in a proton.

(3) The quark-scattering approach predicted that the cross section for producing a jet of hadrons is considerably larger than that for producing a single meson at the same $p_\perp$.[39] For example, the model predicted a jet (quark) to single particle (π^0) ratio of about 370 at $x_\perp = 0.4$ and $\theta_{c.m.} = 90°$. The expectations were in good agreement with subsequent jet trigger experiments.[37,40]

(4) A distinctive feature of the model was that high-$p_\perp$ particles are not isolated but members of a cluster (jet) of particles representing the fragmentation of the quark. In single-particle triggers, one expected to see the remainder of the jet as an enhancement of associated particles in roughly the same direction as the trigger. With one additional assumption[2,41] about the character of fragmentation, the number of particles accompanying a large-$p_\perp$ trigger could be successfully understood.

(5) There is now considerable experimental support for the overall four jet structure shown in Fig. 1 for a large-$p_\perp$ event. These agreements between the quark scattering approach and experi-
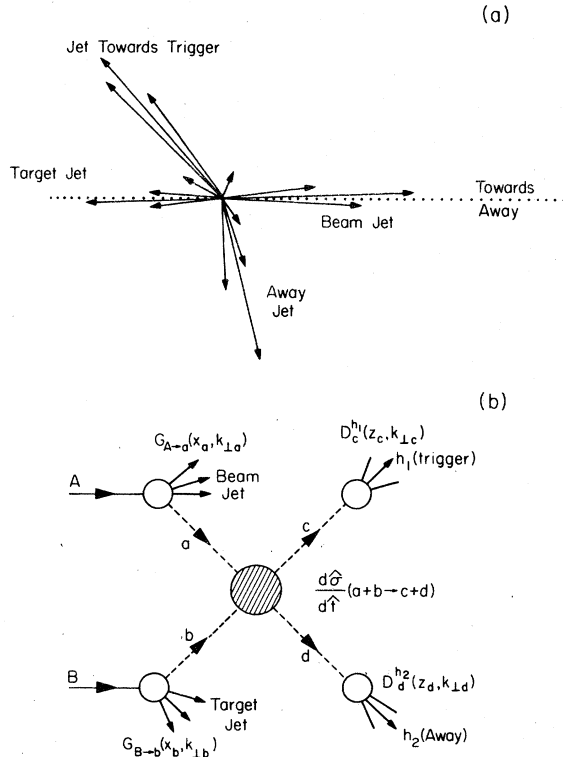
FIG. 1. (a) Illustration of the four-jet structure resulting from a beam hadron (entering at left along dotted line) colliding with a target hadron (entering at right along dotted line) in the c.m. frame: two jets with large $p_\perp$ (collection of particles moving roughly in the same direction), one called the "toward" (trigger) side and one on the "away" side; and two jets with small $p_\perp$ that result from the breakup of the beam and target hadrons (usually referred to as the "soft hadronic" background). (b) Illustration of the underlying structure of the large-$p_\perp$ process $A + B \to h_1 + h_2 + X$. The large-$p_\perp$ trigger hadron h_1 occurs as the result of a large-angle scattering of constituents $(q_a + q_b \to q_c + q_d)$, followed by the decay or fragmentation of constituent c into a towards-side jet of hadrons (one being the trigger h_1) and constituent d into an away-side jet of hadrons (one being h_2). The quantities x_a, x_b, $k_{\perp a}$, $k_{\perp b}$ are the longitudinal fraction of the incoming hadrons A, B momentum and perpendicular momentum of constituents a, b and z_c, z_d $k_{\perp c}$, $k_{\perp d}$ are the fraction of the outgoing constituents longitudinal momentum and perpendicular momentum carried by the detected hadrons h_1 and h_2.

ment indicate strongly that quarks play an important role in the production of high-$p_\perp$ mesons. In particular, they show that the mesons responsible for high-$p_\perp$ triggers probably arise from quarks that have fragmented in a manner similar to that observed in lepton-initiated processes.

B. Failures

As noted in the Introduction, the quark scattering black-box model does not agree in detail with all the results of high-$p_\perp$ experiments. It disagrees with data in the following ways.[38]

(1) Large-$p_\perp$ events are far less coplanar than first expected from a two-to-two scattering subprocess as shown in Fig. 1. Our first guess[2,41] that $\langle k_\perp \rangle_{h \to q} \approx \langle k_\perp \rangle_{q \to h} = 330$ MeV resulted in a too narrow away-side P_{out} distribution. Even our final choice in FFF of $\langle k_\perp \rangle_{h \to q} = 500$ MeV yields more coplanarity than seen in recent experiments.

(2) The quark-quark scattering model predicts too many high-$p_\perp$ particles on the away-side of a large-$p_\perp$ trigger. For example, the number of away hadrons with $z_b \geq 0.5$ (Ref. 42) for a $p_\perp$ $= 4.5$ GeV/c trigger at $\theta = 45°$ and $W = 53$ GeV is predicted in FFF to be 3-4 times larger than seen experimentally by the CCHK group.[15]

(3) Not only does the model predict too many away-side particles, it predicts many more positives than negatives on the away side. For a trigger $p_\perp$ of 3.0 GeV/c, $\theta_{c.m.} = 90°$ and $W = 53$ GeV/ c, the model predicts about 50% more positives than negatives on the away side with $p_\perp$ (away) > 1.5 GeV/c. Recent data from the CERN ISR (Ref. 43) show about equal away-side positives and negatives under these ciruumstances. These are serious problems for the model. The last two imply that (at the small-$x_\perp$ values probed by ISR experiments) the recoiling away-side parton does not fragment in a manner similar to that observed by lepton experiments. Furthermore, as discussed in FFF Table 4, we cannot simply increase $\langle k_\perp \rangle_{h \to q}$ to improve our agreement with (1) and (2). The value of 500 MeV was as large as we could take in FFF without spoiling our agreement with the energy dependence of the single-particle cross section. We feel that it is not useful at present to try to "fiddle" the quark scattering model to make it agree with recent experiments, particularly since there is an emerging candidate theory of strong interactions that apparently has the features necessary to repair the failures of the black-box model.

III. THE INGREDIENTS TO THE QCD APPROACH

A. Effective coupling $\alpha_s(Q^2)$

The effective strong-interaction coupling constant falls logarithmically with increasing Q^2, where Q is some characteristic momentum in a collision. In general, the effective quark-quark-gluon coupling is expected to have the form

$$\alpha_s(Q^2) \equiv \frac{g^2}{4\pi} = \frac{12\pi}{(33 - 2n_f)[\ln(Q^2/\Lambda^2) \pm C]}, \quad (3.1)$$

where n_f is the number of quark flavors (we use $n_f = 4$). The constant C represents corrections that, in general, differ from process to process

but can, in principle, be calculated (although this might be quite difficult in practice).[44] The quantity Λ is an unknown scale factor that can be determined from the amount of "scale breaking" observed in a given experiment. Analysis of the scale breaking in ep and μp collisions indicates that Λ is in the range 0.3 to 0.7 GeV/c (with $C=0$).[17-20]

For ep collisions, Q is the four-momentum transfer from the electron to the quark. On the other hand, the correct kinematic quantity to use for Q^2 in the constituent subprocess shown in Fig. 1 is not known. This problem is, of course, related to the unknown $\pm C$ in (3.1). For definiteness, we will take $C = 0$ and choose

$$Q^2 = 2\hat{s}\hat{t}\hat{u}/(\hat{s}^2 + \hat{t}^2 + \hat{u}^2), \qquad (3.2)$$

where $\hat{s}$, $\hat{t}$, and $\hat{u}$ are the usual Mandelstam s, t, and u invariants but for the constituent subprocess. This form for Q^2 is symmetric in $\hat{s}$, $\hat{t}$, and $\hat{u}$ and approaches $-\hat{t}$ in the case $\hat{t} \ll \hat{s}$. This uncertainty in the form for Q^2 and, correspondingly, the lack of knowledge of $\pm C$ makes predictions at low Q^2 (i.e., low $p_\perp$) in hadron-hadron collisions a bit uncertain.

If the distribution of quarks within the proton, $G_{p \to q}(x)$, and the fragmentation of quarks in hadrons, $D_q^h(z)$, both scale, then the invariant cross section $Ed\sigma/d^3p$ for producing a large-$p_\perp$ meson reflects directly the energy dependence of the quark-quark cross section $d\hat{\sigma}/d\hat{t}$. Thus if the latter behaves as $h(\hat{t}/\hat{s})/\hat{s}^n$, then the former behaves as $f(x_\perp, \theta_{c.m.})/p_\perp^{2n}$. The cross section for the scattering of partons in field theory (see Table I) with $\alpha_s = $ constant yield $2n = N_{\mathrm{eff}} = 4$ where we define

$$N_{\mathrm{eff}} = -\ln(\sigma_1/\sigma_2)/\ln(p_{\perp 1}/p_{\perp 2}), \qquad (3.3)$$

where $\sigma_{1,2}$ is the invariant cross section (at fixed $x_\perp$) at $p_{\perp 1,2}$. Including an α_s that depends on Q^2 according to (3.1) and (3.2) produces an $Ed\sigma/d^3p$ that decreases faster than $1/p_\perp^4$ at small $p_\perp$ ($N_{\mathrm{eff}} \approx 4.8$ for $2 \le p_\perp \le 10$ GeV/c at $x_\perp = 0.2$) but approaches the $1/p_\perp^4$ behavior at large $p_\perp$. This can be seen by the dot-dash curve in Fig. 2 where we plot $p_\perp^8$ times the predicted $Ed\sigma/d^3p$ arising from quark-quark scattering at $x_\perp = 0.2$ versus $p_\perp$ using $\Lambda = 0.4$ GeV/c. One sees that including the $\alpha_s(Q^2)$ dependence brings one a small way toward the flat $(1/p_\perp^8)$ dependence seen experimentally at $p_\perp \lesssim 6$ GeV/c.

B. The quark and gluon distributions $G(x, Q^2)$

In the QCD approach, the "effective" quark distributions in a proton, $G_{p \to q}(x, Q^2)$, do not scale. The influence of this on $\nu W_2(x, Q^2)$ for ep and μp
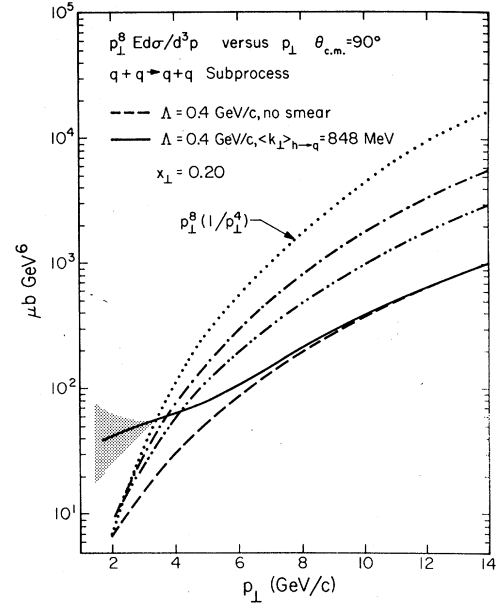

FIG. 2. The behavior of $p_\perp^8$ times the invariant cross section $Ed\sigma/d^3p$ for $pp \to \pi^0 + X$ at $\theta_{c.m.} = 90°$ and $x_\perp = 0.2$ arising from the QCD subprocess $q + q \to q + q$ calculated with $\Lambda = 0.4$ Gev/c. If the quark distributions within protons, $G_{p \to q}(x)$, and the quark fragmentation functions, $D_q^{\pi^0}(z)$, scale and if the strong interaction coupling α_s is constant, then $p_\perp^8 Ed\sigma/d^3p$ behaves like $p_\perp^4$ at fixed $x_\perp$ and $\theta_{c.m.}$ (dotted line). Allowing α_s to depend on Q^2 according to (3.1) yields the dot-dashed curves. Including the expected Q^2 dependence $\alpha_s(Q^2)$ and $G_{p \to q}(x, Q^2)$ results in the dot-dot-dashed curves. Finally, allowing $\alpha_s(Q^2)$, $G_{p \to q}(x, Q^2)$ and $D_q^{\pi^0}(z, Q^2)$ all to vary with Q^2 in a manner expected from QCD results in dashed curve and the solid curve is the result after smearing with $\langle k_\perp \rangle_{h \to q} = 848$ MeV and $\langle k_\perp \rangle_{q \to h} = 439$ MeV. The shaded area represents uncertainties due to the way in which one cuts off the low $\hat{s}$ and $\hat{t}$ singularities in $d\hat{\sigma}/d\hat{t}$. Above $p_\perp \gtrsim 3.5$ GeV/c at $\theta_{c.m.} = 90°$, the results are insensitive to the details of this cutoff procedure.

scattering has been studied[17-20] and may account for the lack of scaling seen in these experiments over the range $4.0 \le Q^2 \le 20.0$ GeV^2. We use the formulation of Ref. 18 to extrapolate these functions to the higher-Q^2 region needed in analyzing high-$p_\perp$ hadron data (see Table II for the range of Q^2 sampled).

In an asymptotically free field theory, scale violations are generated by gluon corrections typified by gluon bremsstrahlung from a quark and by quark-antiquark pair creation by a gluon. One can predict the behavior of the constituent distributions $G_i(x, Q^2)$ given that they are known at some reference momenta Q_0 [large enough so that $\alpha_s(Q_0^2)$ is small enough to make perturbation theory applicable]. Following Ref. 18, the moments of the distributions

TABLE II. The mean values of z_c, Q_x, and Q^2 resulting for $pp \rightarrow \pi^0 + X$ at 90° in the QCD approach with $\Lambda = 0.4$ GeV/c, and where z_c is the fraction of the constituent momenta carried by the trigger hadron (see Fig. 1); Q_x is the component of momentum of the constituent scattering toward the trigger ($Q_x = k_{xa} + k_{xb}$, see Table I and Fig. 2 of FFF); Q^2 is defined by Eq. (3.2).

W (GeV)	$P_\perp$ (GeV/c)	$\langle z_c \rangle$	$\langle Q_x \rangle$ (GeV)	$\langle Q^2 \rangle$ (GeV²)
53	2.0	0.68	1.25	7.9
53	4.0	0.75	0.86	33.7
53	7.0	0.81	0.61	96.5
53	9.0	0.84	0.54	149.0
19.4	1.94	0.74	1.53	4.8
19.4	3.0	0.86	1.77	7.6
19.4	4.0	0.89	1.76	15.5
19.4	6.0	0.92	1.46	42.9
19.4	7.0	0.94	1.46	58.5
500	10.0	0.58	0.16	525
500	30.0	0.69	0.10	3003
1000	10.0	0.53	0.21	751
1000	30.0	0.61	0.10	4184

$$M_i(n, Q^2) = \int_0^1 x^n G_i(x, Q^2) dx \qquad (3.4)$$

are given in terms of the moments at Q_0 by

$$M_j(n, Q^2) = \sum_{i=1}^{9} M_i(n, Q_0^2) R_{ij}(n, Q^2, Q_0^2), \qquad (3.5)$$

where $R_{ij}(n, Q^2, Q_0^2)$ is a known matrix (depending

on Λ) and i corresponds to the constituent types ($u, d, s, c, \bar{u}, \bar{d}, \bar{s}, \bar{c}$, gluon). The final resulting distributions at Q^2 are calculated by inverting (3.4) by an inverse Mellin transform [Eq. (13) of Ref. 18].

Figure 3 shows the predicted Q^2 behavior of $\nu W_2(x, Q^2)$ resulting from an analysis of the ep and μp data. The x dependence of the parton distributions at the reference momentum, $G_i(x, Q_0^2 = 4$ GeV²), was chosen to agree with experiment. Unfortunately, the analysis of ep and μp is relatively insensitive to the input gluon distribution with the proton. We take $xG_1(x, Q_0^2) = xG_{p \rightarrow g}(x, Q_0^2) = (1 + 9x)(1 - x)^4$ at the reference momentum. It integrates to a total momentum for gluons within the proton of 50%. The resulting Q^2 dependence of $G_{p \rightarrow g}(x, Q^2)$ is also shown in Fig. 3. Both $\nu W_2(x, Q^2)$ and $xG_{p \rightarrow g}(x, Q^2)$ exhibit a rise at small x and a decrease at large x as Q^2 increases. The effect is particularly dramatic for the latter.

The QCD interpretation of the ep and μp inelastic-scattering data has some ambiguities because one expects, not only the logarithmic scale breaking shown in Fig. 3, but also other corrections falling more rapidly with Q^2. The latter would be unimportant at very large $Q^2 \gtrsim 50$ (GeV/c)² but are important in the Q^2 range probed by the current data. One example of such a correction is the $O(m^2/Q^2)$ correction (m is proton mass) generated by using x' and not x as the argument of the structure functions. Here
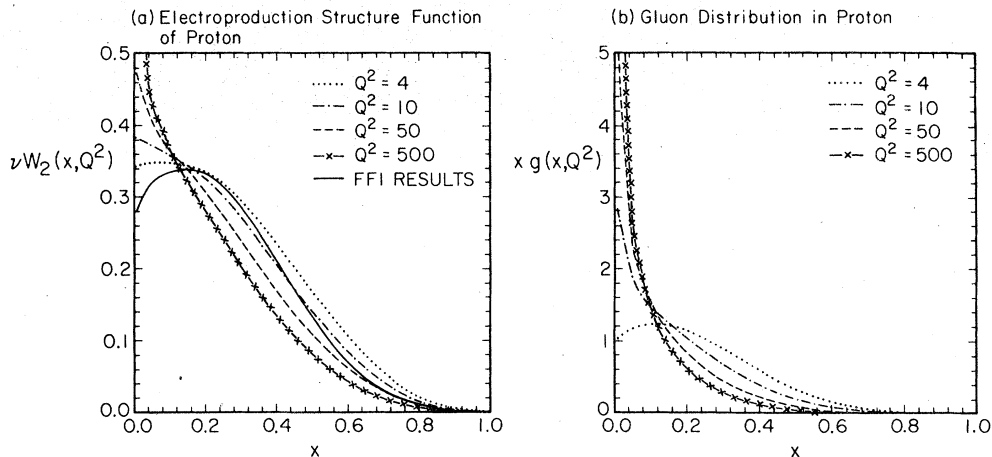
SCALE BREAKING $\Lambda = 0.4$ GeV/c

FIG. 3. (a) The predicted Q^2 dependence (scale breaking) of the electroproduction structure function for the proton $\nu W_2(x, Q^2)$ arising from the constituent (quarks, antiquarks and gluons) distributions $G_i(x, Q^2)$ used in this analysis. The distributions at high Q^2 are calculated from the distributions at the reference momentum $Q_0^2 = 4$ GeV² using a QCD moment analysis with $\Lambda = 0.4$ GeV/c. In asymptotically free theories, one expects a decrease in the number of high-x constituents and an increase in the number of low-x constituents as Q^2 increases. Also shown is the value of $\nu W_2(x)$ (independent of Q^2) used in the quark-quark black box model of FF1. (b) The predicted Q^2 dependence of the distribution of gluons within the proton $xG_{p \rightarrow g}(x, Q^2) = xg(x, Q^2)$ used in this analysis. The distribution at high Q^2 is calculated in terms of a distribution at the reference momentum $Q_0^2 = 4$ GeV² given by $xg(x, Q_0^2) = (1 + 9x)(1 - x)^4$.

$$x' = \frac{x}{1 + m^2 x/Q^2} \sim x - m^2 x^2/Q^2 \,. \qquad (3.6)$$

This leads to scale breaking that is about half the observed amount in the large $x \gtrsim 0.3$ region. However, one can construct variables of a similar type (for instance x_{super} introduced by Atwood[45]) that can describe all the observed large-x scale breaking in terms of $O(m^2/Q^2)$ corrections. Such models give essentially no scale breaking at low x and the important feature of the QCD approach is that the same value of Λ describes the scale breaking at both low and high x. This is shown in Fig. 4. It should be noted that the fit to the low-x data is poorer than that at high x although the trend with Q^2 is given well in both cases. This is because the low-x data is new data that was not available when the parameters of the QCD solution were determined.[46] In Ref. 18, we not only considered structure functions that were a function of x but also a more complicated and probably more realistic formalism developed by Georgi and Politzer.[17] This includes $O(m^2/Q^2)$ terms not only in the argument of the structure functions [similar to (3.6) above] but also as overall multiplicative factors. It turns out that the $O(m^2/Q^2)$ terms tend to cancel among themselves and this formalism is phenomenologically equivalent to the simple formulation we use here. In particular, essentially the same value of $\Lambda \approx 0.5$ GeV/c is found in the best fit of both formalisms.

If one includes the scale-breaking effects of $G_i(x, Q^2)$ in addition to the running coupling constant $\alpha_s(Q^2)$, the resulting $pp \to \pi^0 + X$ cross section arising from the quark-quark subprocess has an N_{eff} equal to about 5.0 and 5.5 for the range $2.0 \leqslant p_\perp \leqslant 10.0$ at $x_\perp = 0.2$ and 0.5, respectively. The scale breaking of $G_i(x, Q^2)$ has little effect at $x_\perp = 0.2$ (see Fig. 2) because at this $x_\perp$ one is sensitive to $G_i(x, Q^2)$ near the values of x that are stationary as Q^2 increases.

C. The fragmentation functions $D_i^h(z, Q^2)$

The experimentally measurable constituent fragmentation functions $D_i^h(z, Q^2)$ (here i refers to a gluon or a $u, d, s, c, \bar{u}, \bar{d}, \bar{s}, \bar{c}$ quark) are expected, in asymptotically free theories, to show scale breaking (Q^2 dependences) similar to that predicted for $\nu W_2(x, Q^2)$.[26, 47] The moments of the fragmentation functions to a given hadron h given by

$$\bar{M}_i^h(n, Q^2) = \int_0^1 z^n D_i^h(z, Q^2) dz \,, \qquad (3.7)$$

are given in terms of the moments at some reference momentum Q_0 by an equation similar to

SCALE BREAKING IN
INELASTIC e, μ SCATTERING
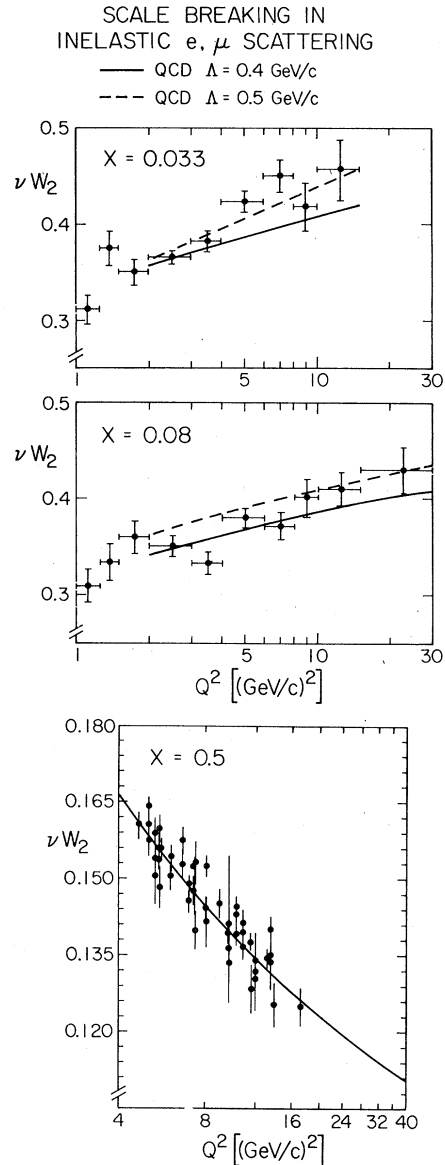—— QCD $\Lambda = 0.4$ GeV/c
--- QCD $\Lambda = 0.5$ GeV/c

FIG. 4. Comparison of the scale-breaking effects (Q^2 dependence) expected from an asymptotically free theory with data on ep and μp inelastic scattering at $x = 0.033$ and 0.08 (Ref. 20) and at $x = 0.5$ (Ref. 72). The theory comes from the analysis of Ref. 18 using $\Lambda = 0.4$ GeV/c (solid curve) and $\Lambda = 0.5$ GeV/c (dashed curve).

(3.6). Namely,

$$\bar{M}_j^h(n, Q^2) = \sum_{i=1}^{9} \bar{M}_i^h(n, Q_0^2) \bar{R}_{ij}(n, Q^2, Q_0^2) \,, \qquad (3.8)$$

where the matrix $\bar{R}_{ij}$ is simply related (but not equal to) R_{ij}.[48] One then uses the Mellin-transform technique of Ref. 18 to invert (3.7) and obtains $D_i^h(z, Q^2)$ in terms of these functions at the reference momentum Q_0^2 (we take $Q_0^2 = 4$ GeV²).

As explained by Gross,[49] the Q^2 dependence of a distribution function depends on its shape at the reference momenta. The faster the function $D(z, Q_0^2)$ falls off with increasing z at large z, the faster the large z points fall as Q^2 is increased above Q_0^2. It is important when considering the fragmentation functions to distinguish the distribution of primary (or direct) mesons from the final net distribution (which includes decay products). The above moment analysis should be applied to the former not the latter. This is, of course, a bit difficult since we do not know experimentally exactly how many resonances are in the quark jets at Q_0^2. What we shall do is to use the results of Ref. 27 (hereafter called FF2) at the reference momentum $Q_0^2 = 4$ GeV^2. The distribution of primary mesons at Q_0^2 is then given by

$$D_q^h(z, Q_0^2) = A_q^h f(1 - z) + B^h \bar{F}(z), \tag{3.9}$$

with A_q^h and B^h given in Table I of FF2 and

$$\bar{F}(z) = F(z) - f(1 - z) \tag{3.10}$$

with

$$f(1 - z) = f(\eta) = 1 - a + 3a\eta^2. $$

The parameter a is chosen to be 0.77 and $F(z)$ is given by Eq. (2.23) in FF2. The distribution of primary mesons in a gluon jet at Q_0^2 is assumed to have the form

$$D_g^h(z, Q_0^2) = B^h F_g(z), \tag{3.11}$$

where we arbitrarily take

$$F_g(z) = 3(1 - z)^2/z, \tag{3.12}$$

where we have assumed, as discussed earlier, that the gluon fragmentation function falls off faster with increasing z than do the quark functions.

We take the primary mesons precisely as explained in FF2 as being either pseudoscalars (π, K, etc.) or vector mesons (ρ, K^*, etc.) with equal likelihood. We use the QCD moment method to calculate the primary meson (pseudoscalar plus vector meson) distributions at any desired Q^2. The resonances are then allowed to decay and we form the total net (direct + indirect) distributions at that Q^2. Typical results are shown in Fig. 5.

The effect on the predicted large-$p_\perp$ invariant cross section of including scale violations of the fragmentation functions is that the N_{eff} now becomes 5.8 and 6.4 between $p_\perp = 2$ and 10 GeV/c at $x_\perp = 0.2$ and 0.5, respectively. Large-$p_\perp$ results are particularly sensitive to scale violations of the $D(z, Q^2)$ function since these violations are largest at high z (see Fig. 5) and this is precisely the region sampled by the calculations.
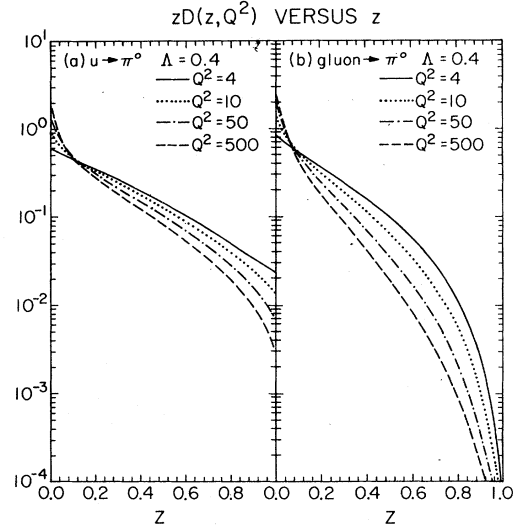

FIG. 5. The Q^2 dependence of the fragmentation function for a u quark to a π^0, $D_u^{\pi^0}(z, Q^2)$, expected from an asymptotically free theory. The distributions at high Q^2 are claculated from the distribution at the reference momentum $Q_0^2 = 4$ GeV^2 using $\Lambda = 0.4$ GeV/c, where D_q^h (z, Q_0^2) is taken from the analysis in FF2. (b) Same as (a) but for the gluon fragmentation function $D_g^{\pi^0}(z, Q^2)$.

D. Transverse momentum

As we learned in FFF, constituents have a large internal transverse momentum inside the proton. Such effects (called smearing) are particularly important for large-$p_\perp$ calculations, due to the "trigger bias" which selects the configuration in which the initial quarks (or gluons) are already moving toward the trigger[11-15,41] (see Fig. 3 of FFF). In QCD, this transverse momentum of the partons can arise from two sources illustrated in Fig. 6.

Firstly, in a proton beam, quarks are confined in the transverse direction to within the proton radius. Therefore, from the uncertainty principle, they must have some transverse momentum. This momentum is intrinsic to the basic parton "wave function" inside the proton. As illustrated in Fig. 6(a), one might expect the wave function to have a term where the trigger parton $k_\perp$ is balanced by another constituent (or constituents) which has the opposite $k_\perp$ and most of the remaining longitudinal momentum. Consider now the plane formed by the beam, target, and a 90° trigger hadron (called the x-z plane in Fig. 6). Typically, the trigger arises from the fragmentation of a constituent with $k_{\perp x} > 0$ which is balanced by the remaining constituents having $k_{\perp x} < 0$. One expects to see this negative $k_{\perp x}$ as a shift in the beam and target jets at large $|x_\parallel|$. This shift (i.e., nonzero $\langle k_{\perp x} \rangle$) of the beam jet as one in-

(a) Type I : $k_\perp$ Intrinsic to Wavefunction

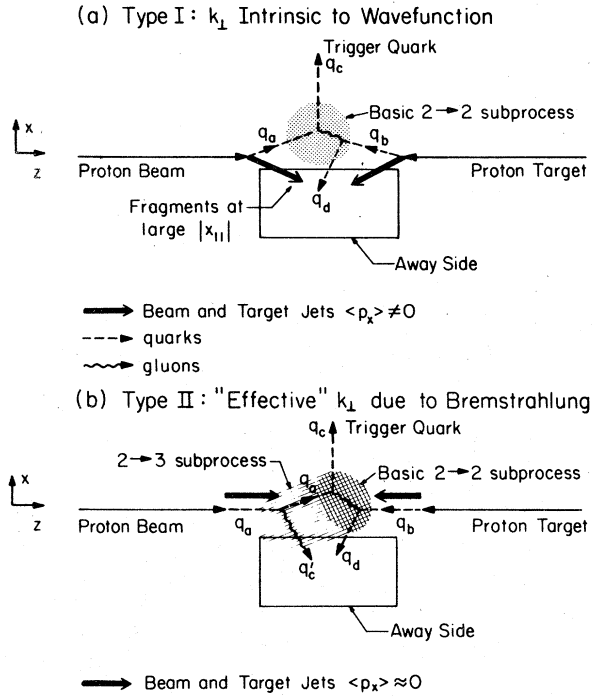(b) Type II : "Effective" $k_\perp$ due to Bremsstrahlung

FIG. 6. (a) Illustration of the nonperturbative component of the transverse momentum of quarks within proton that is intrinsic to the wave function of the proton. One expects this transverse momentum to be balanced by the remaining constituents in the proton which can, in turn, fragment into particles at high $x_{\parallel}$. The away-side consists of the recoiling quark q_d and two slightly shifted jets, one from the beam and one from the target. (b) Illustration of the perturbative component to the transverse momentum of a quark with a hadron which is due to the bremsstrahlung of a gluon before the basic $2 \to 2$ scattering occurs. In this case, the trigger quark is balanced by two away-side jets, one from the quark q_d and from the radiated gluon q_c'.

creases the $p_\perp$ of a 90° trigger has recently been observed by the British-French-Scandinavian (BFS) group at ISR[50] (see Fig. 14 or Ref. 22).

Secondly, in QCD, one expects to receive an "effective" $k_\perp$ of quarks in protons due to the bremsstrahlung of gluons. This perturbation term is illustrated in Fig. 6(b). It corresponds to including two particle to three or more particle processes ($2 \to 3$) rather than just the two particle to two particle $2 \to 2$ scatterings. For such subprocesses, the $k_\perp$ of the quark q_a is balanced by a gluon jet on the away side which subsequently fragments into many low-momentum hadrons. In addition, the mean value of the effective $k_\perp$ is expected to depend on the x value of quark q_a and on the Q^2 for the processes. Separating the origin of the transverse momenta into Types I and II as seen in Fig. 6 is a bit artificial since both mechanisms occur simultaneously.
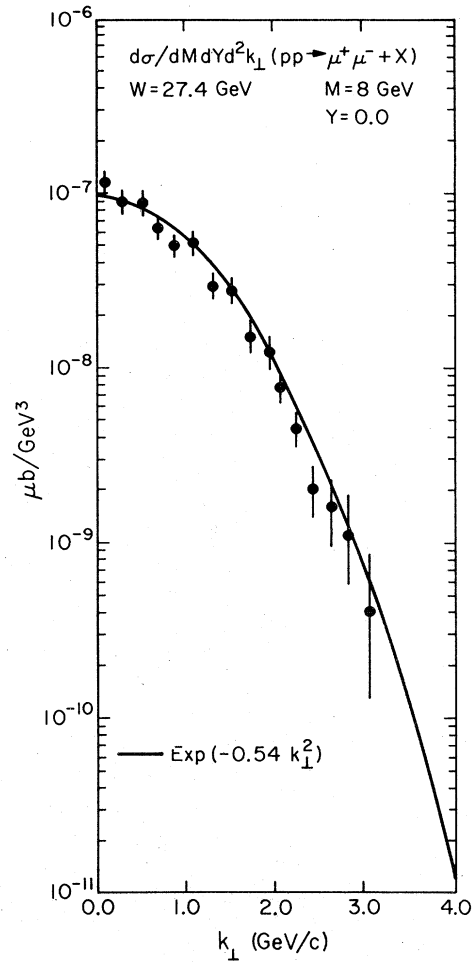

FIG. 7. The transverse-momentum spectrum, $d\sigma/dM dY d^2 k_\perp$, of muon pairs in $p\bar{p}$ collisions at $W = 27.4$ GeV, $M_{\mu\mu} = 8$ GeV, and rapidity $Y = 0$ from Ref. 51. Also shown is a Gaussian fit of the form $\exp(-0.54\, k_\perp^2)$ which yields $\langle k_\perp \rangle_{\mu\mu} \simeq 1.2$ GeV and is interpreted as implying $\langle k_\perp \rangle_{h \to q} = 848$ MeV.

The effective constituent transverse momentum is directly observed in the Drell-Yan process $pp \to \mu^+ \mu^- + X$. Current data[51] indicate that $\langle k_\perp \rangle_{\mu^+ \mu^-}$ is about 1.2 GeV (see Fig. 7). There has been much speculation about how much of the dimuon $k_\perp$ spectra shown in Fig. 7 is due to the wave function (Type I) and how much is explained by QCD perturbation calculations (Type II).[26,30-33] The latter predicts a high-$k_\perp$ tail to the distribution that falls roughly like a power and a mean that depends both on x and Q^2 of the muon pair. For the present analysis, we shall parameterize the transverse momentum of the constituents in protons by a Gaussian with $\langle k_\perp \rangle_{h \to q} = 848$ MeV which produces for the Drell-Yan subprocess the curve shown in Fig. 7. We shall take this distribution to be independent of x and Q^2 and to be the

same for quarks, antiquarks, and gluons in the proton. In so doing, we are not handling properly the x and Q^2 dependence of the high-$k_\perp$ tail expected from QCD bremsstrahlung. At a later date, we hope to calculate and include the $2 \to 3$ processes expected by QCD. For the present, we merely use the data in Fig. 7 to give us an "effective" $k_\perp$ distribution and include only $2 \to 2$ subprocesses.

In a manner similar to that illustrated in Fig. 6, the emission of gluons after the hard-scattering ($2 \to 2$) subprocesses induce an "effective" $k_\perp$ of the hadrons that fragment from the outgoing quarks because one is really seeing two jets rather than one. As for the quark distributions in the proton, we do not include these effects (we also neglect the interferences that arise between the amplitude for emitting gluon before and after the hard $2 \to 2$ process) and for the present take the transverse momentum distribution of hadrons from outgoing quarks (and gluons) to be a Gaussian with $\langle k_\perp \rangle_{q \to h} = 439$ MeV independent of z or Q^2 as in FF2. Again, this is not precisely correct and we hope to improve this in later work.

E. The cross sections $d\hat{\sigma}/d\hat{t}$

In the QCD approach, one includes not only the contributions from quark-quark scattering but also the contributions from quark-gluon and gluon-gluon scattering. We include all seven processes: $qq \to qq$, $\bar{q}q \to \bar{q}q$, $\bar{q}\bar{q} \to \bar{q}\bar{q}$, $gq \to gq$, $g\bar{q} \to g\bar{q}$, $gg \to \bar{q}q$, $\bar{q}q \to gg$, and $gg \to gg$, where g is a gluon. Each $2 \to 2$ differential cross section, $d\hat{\sigma}/d\hat{t}$, is calculated to first order in perturbation theory with an effective coupling constant $\alpha_s(Q^2)$ as in (3.1). These cross sections have been calculated previously by Cutler and Sivers[28] and by Combridge, Kripganz, and Ranft[29] and for completeness are given in Table I.[52] All these cross sections behave as $\hat{s}^{-2}$ at fixed $\hat{t}/\hat{s}$ (and for constant α_s) so that including gluons does not help in changing N_{eff} from 4 to 8 but gluons are important in increasing the magnitude of the low-$x_\perp$ cross section to agree with data.[13,28,29] In addition, we will see that gluons play an important role in understanding the high-$p_\perp$ correlation data.

Including gluons, unfortunately, introduces an uncertainty (at low $x_\perp$) in the high-$p_\perp$ predictions. As explained in Secs. III B and III C, the gluon distribution in a proton and the gluon fragmentation functions are essentially unknown. We only know that the total momentum carried by quarks and gluons in a proton is that of the proton and similarly the total energy carried by all the hadron fragments from a gluon is the gluon energy. Many of our high-$p_\perp$ predictions depend on these unknown distributions, for the QCD quark-gluon and

gluon-gluon scattering cross sections are large. If one accepts QCD as the correct description for high-$p_\perp$ processes, then one could eventually hope to use the hadron-hadron data to help determine these functions. For the present, we simply calculate with our initial guesses for $G_{p \to g}(x, Q_0^2)$ and $D_g^h(z, Q_0^2)$ and do not attempt to find the optimal forms for these functions by fitting high-$p_\perp$ data.

As discussed in great detail in FFF, cross sections of the type given in Table I are not adequate once one allows for a nonzero transverse momentum of constituents in the hadrons or of hadrons from in the outgoing jets.[53] This is because they diverge at $\hat{s}$, $\hat{u}$, or $\hat{t}$ equal zero which can occur once $\langle k_\perp \rangle_{h \to q}$ or $\langle k_\perp \rangle_{q \to h}$ is nonzero. To remove this unwanted singularity in the integral, we simply replace $\hat{s}$, $\hat{t}$, and $\hat{u}$ in Table I by $\hat{s} + M_0^2$, $M_0^2 - \hat{t}$, and $M_0^2 - \hat{u}$, respectively, with $M_0^2 = 1.0$ GeV^2.[54] Because we are generating the transverse momentum of the constituents by a Gaussian, the results for hadron production at large $p_\perp$ are not sensitive to this ad hoc cutoff procedure. With the large-$k_\perp$ damping, characteristic of a Gaussian, once one has removed the infinity at say $\hat{t} = 0$ (by whatever means), one never samples this low-$\hat{t}$ region when calculating high-$p_\perp$ meson production. This would not be true for a transverse-momentum distribution falling off less rapidly with $k_\perp$ (for example, like a power) so that the large-$k_\perp$ tails expected by the QCD processes in Fig. 6 will have to be handled differently in the future.

Because $\langle k_\perp \rangle_{h \to q}$ is large, one does begin to become sensitive to the low-$\hat{s}$ and -$\hat{t}$ cutoff at low $p_\perp$. This is illustrated in Fig. 2 where we show the results for $pp \to \pi^0 + X$ at $x_\perp = 0.2$ and $\theta_{\text{c.m.}} = 90°$ arising from quark-quark scattering before and after smearing. The shaded area represents uncertainties due to varying the low-$\hat{s}$ and -$\hat{t}$ cutoffs. The region of $p_\perp \lesssim 3.5$ GeV/c cannot, at present, be used to quantitatively test the QCD ideas since this region is sensitive to the cutoff procedure.[55] For $p_\perp \gtrsim 3.5$ GeV/c, on the other hand, the manner of cutoff is not important and the result depends only on the amount of smearing (i.e., on $\langle k_\perp \rangle_{h \to q}$).

IV. RESULTS

A. The single-particle cross section

1. $p_\perp^{-8}$ behavior

Figure 8 shows a comparison of the predicted and experimental behavior of $p_\perp^8$ times $E d\sigma/d^3p$ for $pp \to \pi + X$ at $\theta_{\text{c.m.}} = 90°$ and $x_\perp = 0.2$, 0.35, and 0.5 versus $p_\perp$. The dot-dashed and solid curves are the final results before and after smearing, respectively, with $\Lambda = 0.4$ GeV/c. The dashed
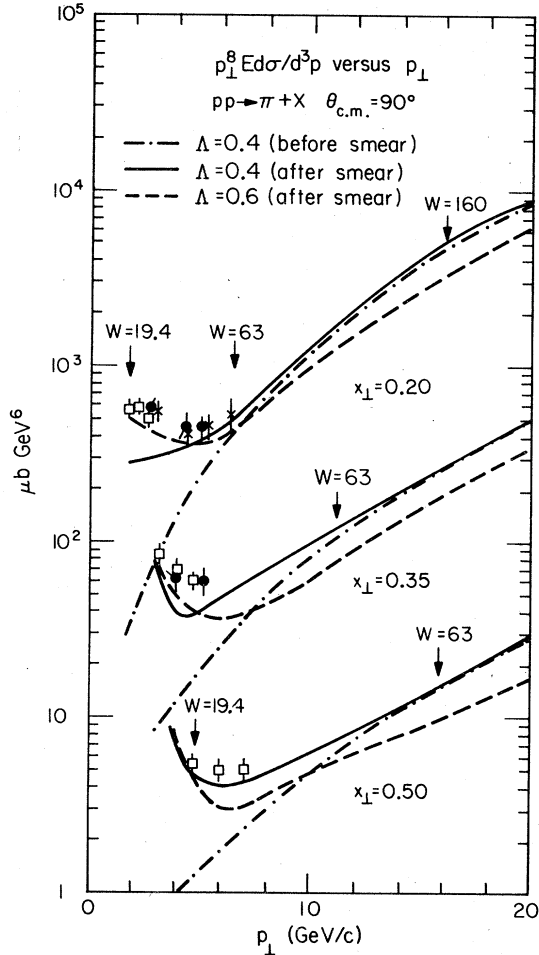
FIG. 8. The data on $p_\perp^8$ times $Ed\sigma/d^3p$ for large $p_\perp$ pion production at $\theta_{c.m.}=90°$ and *fixed* $x_\perp=0.2$, 0.35, and 0.5 versus $p_\perp$ (open squares: Ref. 73, solid dots: Ref. 74, crosses: Ref. 75) compared with the predictions (with absolute normalization) of a model that incorporates all the features expected from QCD. The dot-dashed and solid curves are the results before and after smearing, respectively, using $\Lambda=0.4$ GeV/c and the dashed curves are the results using $\Lambda=0.6$ GeV/c (after smearing).

FIG. 9. The same as Fig. 8 except we now plot $p_\perp^4$ times $Ed\sigma/d^3p$ versus $p_\perp$ at $x_\perp=0.2$ and $\theta_{c.m.}=90°$. One clearly sees the asymptotic approach to an $Ed\sigma/d^3p \propto p_\perp^{-4}$ behavior at fixed $x_\perp$.

curves are the results (after smearing) using $\Lambda=0.6$ GeV/c. The effect of smearing (at fixed $x_\perp$) is to increase the low-$p_\perp$ predictions (by about a factor of 10 at $p_\perp=2$ GeV/c and $x_\perp=0.2$) while not affecting much the high-$p_\perp$ region. For the range $2.0 \leqslant p_\perp \leqslant 6.0$ GeV/c at $x_\perp=0.2$, and $4.0 \leqslant p_\perp \leqslant 10.0$ GeV/c at $x_\perp=0.5$, the results are roughly independent of $p_\perp$ (when multipled by $p_\perp^8$). However, this $p_\perp^{-8}$ behavior is only a "local" effect. It holds only over a small range of $p_\perp$ (at low $p_\perp$); the region depending somewhat on $x_\perp$. As $p_\perp$ increases, the predictions approach the expected $p_\perp^{-4}$ behavior. This can be seen more clearly in Fig. 9 where we plot the predictions and
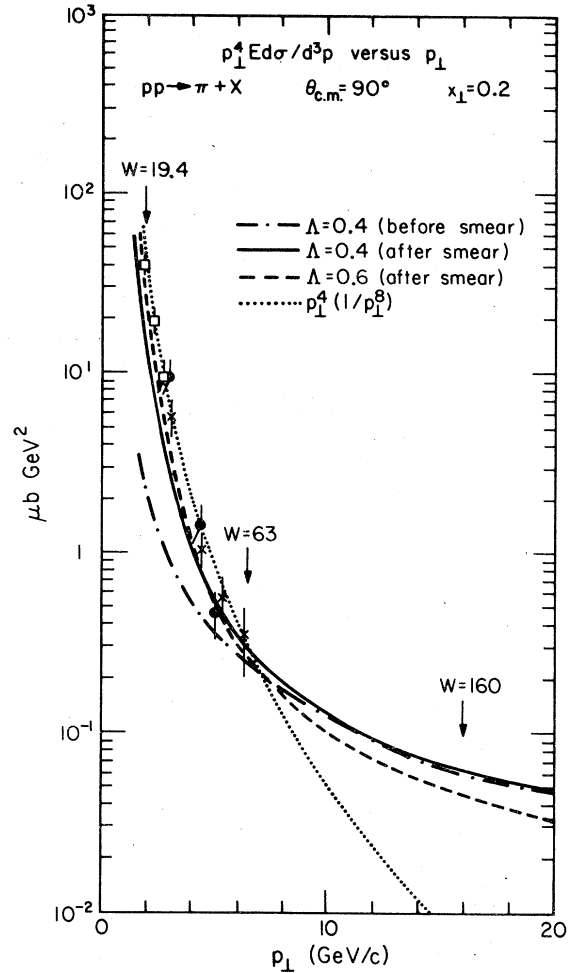
data times $p_\perp^4$ at $x_\perp=0.2$ and $\theta_{c.m.}=90°$. The behavior becomes $p_\perp^{-4}$ only asymptotically, but by $p_\perp=10$ GeV/c at this $x_\perp$, it is fairly close (about $p_\perp^{-5}$).

As illustrated in Fig. 2, the low-$p_\perp$ region is sensitive to the small-$\hat{s}$ and $-\hat{t}$ cutoff employed.[55] However, because of the Gaussian falloff of the transverse momentum distributions, the results are completely insensitive to the form of the cutoff for $p_\perp \gtrsim 3.5$ GeV/c at $\theta_{c.m.}=90°$. For example, Table II shows that the constituent subprocess has a mean momentum $\langle Q_x \rangle = 1.76$ GeV/c for a $p_\perp=4$ GeV/c trigger at $W=19.4$ GeV but even for this large "trigger bias", only 12% of the total $pp \to \pi^0 +X$ cross section arises from the region $|\hat{t}| < 10$ GeV^2 and none arises for $|\hat{t}| < 5$ GeV^2.

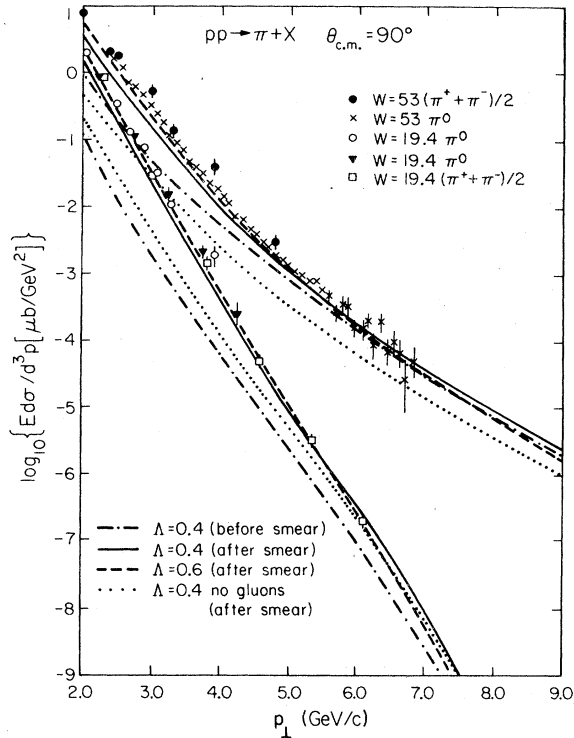The data on $Ed\sigma/d^3p$ at *fixed* $W=19.4$ and 53 GeV versus $p_\perp$ are compared with the theory in

FIG; 10. Comparison of a QCD model (normalized absolutely) with data on large-$p_\perp$ pion production in proton-proton collisions as $W = \sqrt{s} = 19.4$ and 53 GeV/c with $\theta_{c.m.} = 90°$ (open squares: Ref. 73, solid dots: Ref. 74, crosses: Ref. 75, solid triangles: Ref. 76, open circles: Ref. 77). The dot-dashed and solid curves are the results before and after smearing, respectively, using $\Lambda = 0.4$ GeV/c and $\langle k_\perp \rangle_{h \to q} = 848$ MeV and the dashed curves for $\Lambda = 0.6$ GeV/c (after smearing). The contribution arising from quark-quark, quark-antiquark, and antiquark-antiquark scattering (i.e., no gluons) is shown by the dotted curves (after smearing).

Fig. 10. The agreement is quite remarkable. It is almost as good as the black-box model (Fig. 13 of FF1) where we chose the behavior of $d\hat\sigma/d\hat t$ and the normalization to fit the data. The results before smearing are also shown (dot-dashed curves). Smearing has little effect for $p_\perp \geqslant 4.0$ GeV/c at $W = 53$ GeV but has a sizable effect (even at $p_\perp = 6.0$ GeV/c) at $W = 19.4$ GeV due to the steepness of the cross section at this low energy. The contributions to the total invariant cross section from quark-quark elastic scattering (plus $q\bar q \to q\bar q$ and $\bar q\bar q \to \bar q\bar q$) are shown in Fig. 10 (dotted curve). Gluons make important contributions to the cross section at small $x_\perp$ ($x_\perp \lesssim 0.4$).

We cannot at this time say whether the slight disagreement in the normalization of the theory seen in Figs. 8, 9, and 10 at low $x_\perp$ (about a factor of 2 at $p_\perp = 2$ GeV/c and $W = 53$ GeV) is significant. At these low values of $x_\perp$ and $p_\perp$, the theory cannot

at present be calculated precisely as the results depend sensitively on the unknown gluon distributions, the shape of the transverse-momentum distributions of the quark within the hadrons, the nature of the low-$\hat s$ and -$\hat t$ cutoff, our choice for Q^2, and possibly higher-order corrections [such as the $\pm C$ in Eq. (3.1)]. It may be that all of the invariant cross section down to $p_\perp$'s as low as 1.5 or 2.0 GeV/c is due to the scattering of quarks and gluons as described by QCD. On the other hand, it may be that other nonleading constituent subprocesses such as the ones estimated by Blankenbecler, Brodsky, and Gunion[56] make some contributions in the range of $1.5 \lesssim p_\perp \lesssim 4.0$ GeV/c with QCD dominating at the higher $p_\perp$'s.

2. Angular dependence

In FF1 we used the data shown in Fig. 11 to deduce that $d\hat\sigma/d\hat t \propto 1/\hat s \hat t^3$ was the preferred form for the angular dependence of quark-quark scattering. We must now see if the QCD predictions are
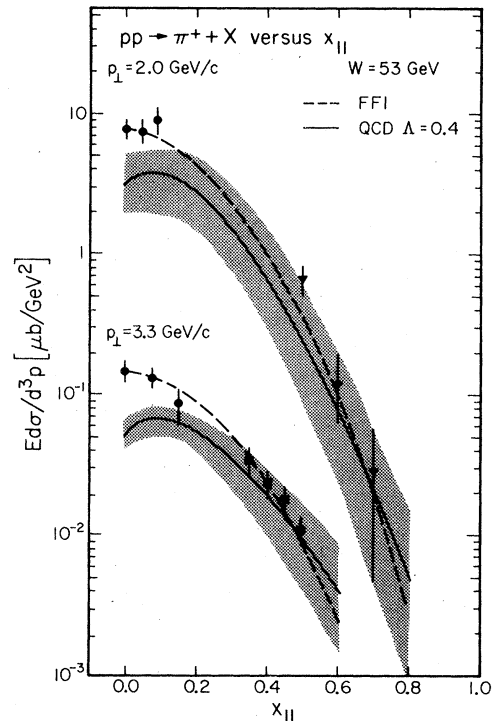

FIG. 11. Data on the $x_\parallel$ dependence of the invariant cross section for $pp \to \pi^+ + X$ at $W = 53$ GeV and $p_\perp = 2.0$ and 3.3 GeV/c (solid dots: Ref. 74, solid triangles: Ref. 78, solid Squares: Ref. 79) compared with the results of a QCD model with $\Lambda = 0.4$ GeV/c (solid curves). At these low-$p_\perp$ values, the predictions are sensitive to the low $\hat s$ and $\hat t$ cutoff of $d\hat\sigma/d\hat t$. At any fixed $p_\perp$, the uncertainty due to the cutoff procedure (illustrated by the shaded areas) is greater at large $x_\parallel$. Also shown (dashed curves) are the results from the quark-quark black-box model of FF1 which was adjusted to fit these data.
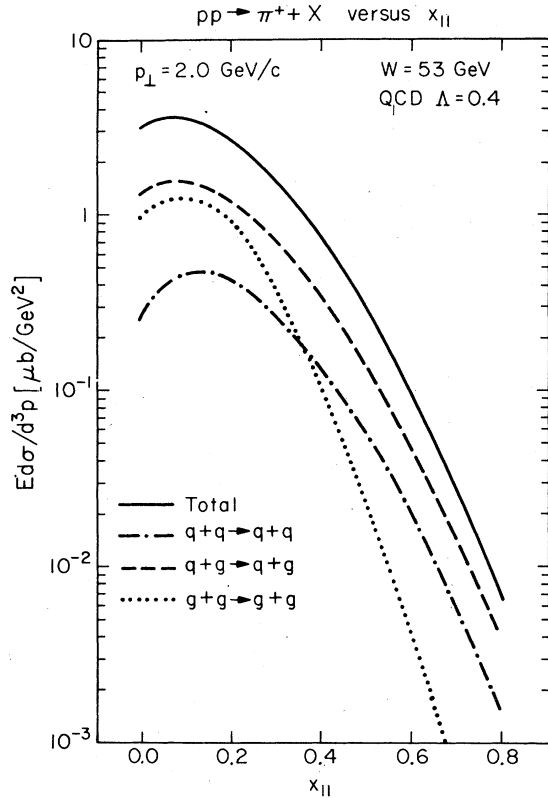
pp → π⁺ + X   versus x∥

FIG. 12. Contributions to the total $Ed\sigma/d^3p$ for $pp \to \pi^+$ $+ X$ arising from the various QCD subprocesses, $q + q \to q$ $+ q$, $q + g \to q + g$, and $g + g \to g + g$ at $W = 53$ GeV, $p_\perp = 2.0$ GeV/c versus $x_\parallel$.

consistent with the same data. Figure 11 shows the QCD results with $\Lambda = 0.4$ GeV/c (after smearing) for the $x_\parallel$ dependence of $Ed\sigma/d^3p$ for pp $\to \pi^+ + X$ at $p_\perp = 2$ and 3.3 GeV/c and $W = 53$ GeV. As noted earlier, the predictions are a bit low at this low $p_\perp$; however, the QCD $x_\parallel$ dependence is not in gross disagreement with the data. Unfortunately, comparison with these low-$p_\perp$ data is not very significant. First, with the large value of $\langle k_\perp \rangle_{h \to q}$ we are now using, the results for these $p_\perp$ values are sensitive to the manner in which we remove the singularity in $d\hat{\sigma}/d\hat{t}$ at $\hat{t}$ (or $\hat{u}$) equal zero. This is particularly true at large $x_\parallel$ where the constituent scattering occurs at small $\hat{t}$ (or $\hat{u}$) values. We have tried to indicate this uncertainty by the shaded region in Fig. 10. Secondly, since this region is so sensitive to smearing, the results depend on our assumption that $\langle k_\perp \rangle_{h \to q}$ is independent of the x_q of the quark q. Modifying this assumption could change the resulting $x_\parallel$ dependence.

Furthermore, in the QCD approach, the $x_\parallel$ dependence of the invariant cross section does not directly reflect the angular dependence of $d\hat{\sigma}/d\hat{t}$.

Figure 12 shows that the various QCD subprocesses have differing $x_\parallel$ dependences so that the result depends not only on the various $d\hat{\sigma}/d\hat{t}$ but also on the amount of each term. For example, the gluon-gluon scattering contributions fall off fast with increasing $x_\parallel$. We could cause the predicted $Ed\sigma/d^3p$ to fall off more rapidly with $x_\parallel$ by increasing the amount of gluon-gluon scattering [by changing the relatively unknown functions $G_{p \to g}(x, Q^2)$ and $D_g^{\pi^+}(z, Q^2)$].

3. Particle ratios

As mentioned earlier, and as shown in Fig. 10, gluons make an important contribution to the single-particle invariant cross section at low $x_\perp$. However, since the gluon fragmentation function has been chosen to be considerably smaller at large z than the quark fragmentation function, an experiment demanding a large-$p_\perp$ meson trigger is "biased" in favor of the toward-side constituent being a quark rather than a gluon. Table III gives the fraction of the single-particle cross section arising from the various combinations of toward and away constituents. At $W = 53$ and $p_\perp \gtrsim 4.0$ GeV/c, 45% of the π^0 cross section arises from a toward-side quark having scattered off a recoiling gluon while 27% arises from the quark recoiling off another quark (a total of 72%). Tables III and IV show that for $x_\perp \gtrsim 0.3$, the toward constituent for single-particle triggers is almost always a quark. This quark, however, scatters off both quarks and gluons in the other proton so that the recoiling constituent is quite often a gluon. At $W = 53$ GeV, a π^0 trigger with $p_\perp = 4.0$ GeV/c, the toward constituent is a quark (or antiquark) 72% of the time while the away constituent is a gluon 62% of the time.

This "bias" for quarks rather than gluons in single-particle triggers means that the predictions for ratios of different kinds of particles will not be very different from those of the quark-quark scattering black-box approach. As shown in Fig. 13, $pp \to (\pi^+/\pi^-) + X$ ratio predictions of QCD are smaller due to the contamination from the gluon decays (gluons fragment into equal numbers of positives and negatives). They are in equally good agreement with data. The QCD particle ratios do not "scale" as did the FF1 results (i.e., they are a function of $x_\perp$ and W at fixed $\theta_{c.m.}$). The curve displayed in Fig. 13(a) is calculated at $W = 19.4$ GeV and increases slightly as W increases (by about 20% in going from $W = 19.4$ to 53 GeV/c).

B. The jet cross section

The "bias" in favor of toward-side quarks does not occur when one triggers on jets rather than

TABLE III. Fraction of the total $pp \to \pi^0 + X$ 90° invariant cross section arising from various combinations of toward-side (trigger) and away-side partons. Results are shown for the cases where the π^0 trigger came from a quark or gluon and the recoiling constituent (away-side) is a quark or gluon or either (sum). The notation is "toward → away" and "quark" refers to $q + \bar{q}$.

W (GeV)	$P_\perp$ (GeV/c)	$x_\perp$	Toward-side quark			Toward-side gluon		
			quark → quark	quark → gluon	quark → anything	gluon → quark	gluon → gluon	gluon → anything
53	2.0	0.08	0.16	0.41	0.57	0.15	0.28	0.43
53	4.0	0.15	0.27	0.45	0.72	0.11	0.17	0.28
53	7.0	0.26	0.39	0.48	0.87	0.07	0.06	0.13
53	9.0	0.34	0.45	0.48	0.93	0.04	0.03	0.07
19.4	1.94	0.20	0.18	0.36	0.54	0.15	0.31	0.46
19.4	3.0	0.31	0.27	0.54	0.81	0.08	0.11	0.19
19.4	4.0	0.41	0.37	0.52	0.89	0.06	0.05	0.11
19.4	6.0	0.62	0.55	0.42	0.97	0.02	0.01	0.03
500	10	0.04	0.24	0.32	0.56	0.15	0.29	0.44
500	30	0.12	0.34	0.42	0.76	0.13	0.11	0.24

on single particles and, as can be seen in Table IV, gluons make up a sizable fraction of the total jet cross section. With our guesses for the gluon distributions, gluons are responsible for 73% of the jet triggers at $p_\perp = 4$ GeV/c, $W = 53$ GeV, and $\theta_{c.m.} = 90°$. Even at higher-$x_\perp$ values such as $p_\perp = 6.0$ GeV/c, $W = 19.4$ GeV, $\theta_{c.m.} = 90°$, gluons still make up 45% of the jets. Because of the presence of gluon jets and because the quark fragmentation functions $D_q^h(z, Q^2)$ are smaller at high z due to scale-breaking effects, the jet to single-π^0 ratio is now predicted to be larger than it was for the quark-quark black-box approach. This is seen in Fig. 14 where we plot the invariant cross section for $pp \to \text{Jet} + X$ divided by $pp \to \pi^0 + X$ at $\theta_{c.m.} = 90°$ versus $x_\perp$. In the QCD approach, this ratio no longer "scales." It is a function not only of $x_\perp$ (at fixed $\theta_{c.m.}$), but also of W. We show results for $W = 19.4$, 53, and 500 GeV.

As noted in Ref. 57, the quark scattering model in FF1 and FFF agreed quite well with the jet cross section observed experimentally at $W = 19.4$ GeV and $3 \leqslant p_\perp \leqslant 6.0$ GeV/c. We might now be concerned that the QCD results for the jet cross section are larger than FF1 by a factor of about 5 in this region. We have, however, previously been somewhat naive when comparing theory with experiment. What we show in Fig. 14 is the cross section for producing a quark (or gluon) with a given momentum (divided by the π^0 cross section at the same momentum). However, as we noticed in Ref. 27, quarks of a given momentum (equal to their energy) cannot produce jets with the momentum of all particles equal to the energy of all particles. Our jet model in FF2 gives $E_{tot} - p_{z_{tot}} \approx 1.2$ GeV for quark jets. Since the cross section for producing jets falls so steeply, the cross section for producing a jet with a given $p_{z_{tot}}$ is considerably smaller than that for producing one with a given E_{tot}. As explained in Ref. 41, it is the former that is more closely connected to what is measured experimentally. At $W = 19.4$ GeV/c, we estimate that the cross section to produce a jet where $p_{z_{tot}} = 5$ GeV/c at 90° is about 10 times smaller than the cross section to produce a jet whose $E_{tot} = 5$ GeV/c. If we correct for this effect, the new QCD prediction at $W = 19.4$ GeV is within a factor of 2 of the old (incorrectly interpreted) FF1 results that appeared to agree so well with the data.

The difference between E_{tot} and $p_{z_{tot}}$ of a jet arises, of course, from low-momentum particles that have energy due to their mass (or $k_\perp$) but have little momentum p_z. This is tangled with the experimental uncertainty in all hadron-jet experiments concerning low-$p_\perp$ particles. One cannot be sure that one is not losing the low-$p_\perp$

TABLE IV. Fraction of the $pp \to \pi^0 + X$ and $pp \to$ jet $+X$ cross section at $\theta_{c.m.} = 90°$ arising from the case where the toward-side (or trigger) constituent is a u, d, or antiquarks $\bar{Q} = \bar{u} + \bar{d} + \bar{s}$ or a gluon. Also shown is the fraction arising from the case where the recoiling or away side constituent is a u, d, or antiquarks $\bar{Q}$ or a gluon.

W (GeV)	$P_\perp$ (GeV/c)	Trigger	Toward side				Away side			
			u	d	$\bar{Q}$	Gluon	u	d	$\bar{Q}$	Gluon
53	2	π^0	0.20	0.20	0.13	0.43	0.14	0.09	0.06	0.70
53	2	jet	0.12	0.10	0.14	0.64	0.18	0.09	0.08	0.63
53	4	π^0	0.36	0.25	0.09	0.27	0.23	0.09	0.05	0.62
53	4	jet	0.12	0.09	0.05	0.73	0.20	0.08	0.02	0.69
53	7	π^0	0.55	0.26	0.05	0.13	0.28	0.14	0.05	0.53
19.4	3.0	π^0	0.46	0.29	0.06	0.19	0.20	0.11	0.03	0.66
19.4	3.0	jet	0.13	0.08	0.04	0.74	0.21	0.08	0.02	0.68
19.4	6.0	π^0	0.73	0.24	0	0.03	0.42	0.15	0	0.43
19.4	6.0	jet	0.37	0.17	0	0.45	0.36	0.14	0	0.50
500	10	π^0	0.18	0.17	0.18	0.44	0.21	0.08	0.09	0.60
500	10	jet	0.05	0.05	0.06	0.81	0.13	0.11	0.07	0.66
500	30	π^0	0.37	0.23	0.14	0.24	0.29	0.12	0.05	0.53
500	30	jet	0.11	0.08	0.10	0.69	0.21	0.11	0.06	0.60

jet particles that are not well collimated or gaining low-$p_\perp$ background from the beam and target jets in Fig. 1. Only by doing a very careful analysis, including the precise acceptances of a given experiment, can one distinguish between the results of FF1 and the new QCD approach in spite of their rather large differences. One might hope someday to distinguish experimentally between gluon and quark jets. The gluon jets are assumed to have a higher multiplicity of particles each with lower momentum on the average. In addition, unlike the quark jets discussed in Ref. 27, gluon jets will carry on the average no net charge (or strangeness, etc.).

C. The toward-side correlations

The jet physics, discussed in the previous subsection, directly tests that particles at high $p_\perp$ are not produced singly but, rather, are members of a cluster. This aspect of constituent models can also be tested in single-particle triggers by observing the accompanying particles produced near the trigger (in phase space). Experimentally, one observes an enhancement of particles with high $p_\perp$ accompanying the high-$p_\perp$ trigger which was predicted correctly from the quark scattering model[2,41] together with an assumption about the double fragmentation function, $D_q^{h_1, h_2}(z_1, z_2)$.[27] In the QCD case, the trigger hadrons usually come from quarks rather than gluons and, furthermore, the mean value of z_c shown in Table II are similar to those in FFF.[58] Thus the new predictions, as

shown in Fig. 15, are, in fact, very similar to the quark scattering results. However, the QCD results have an additional uncertainty due to our lack of knowledge of the gluon double fragmentation functions, $D_g^{h_1, h_2}(z_1, z_2, Q^2)$. In Fig. 15 where 18% of the triggers come from gluons, we have assumed that the accompanying particles were just given by the fragmentation of a gluon with momentum $(1 - z_c)$ times that of trigger gluon. This has the feature of giving the correct multiplicity for the produced hadrons; however, it is surely not exact. For example, for a π^+ trigger, one would expect to find more high-$p_\perp$ π^-'s than π^+'s in the accompanying particles. In Ref. 22, an upper estimate for the effect of the gluon decays was deduced by assuming that the accompanying hadrons came from a $\bar{u}$ (or d) jet carrying all of the remaining momentum. Comparing with the CCHK data, this upper estimate and the lower estimate gotten by dropping gluon term completely roughly bracket the data.

In summary, we find that the QCD calculations have somewhat greater uncertainty than those in FFF coming from the gluon contribution. However, both models are in good agreement with the same-side correlation data.

D. Away-side correlations

1. Away-side multiplicity $n(z_p)$

An important consequence of the QCD approach is that the number of away-side hadrons with large-$p_\perp$ $(-p_x)$ is predicted to be considerably
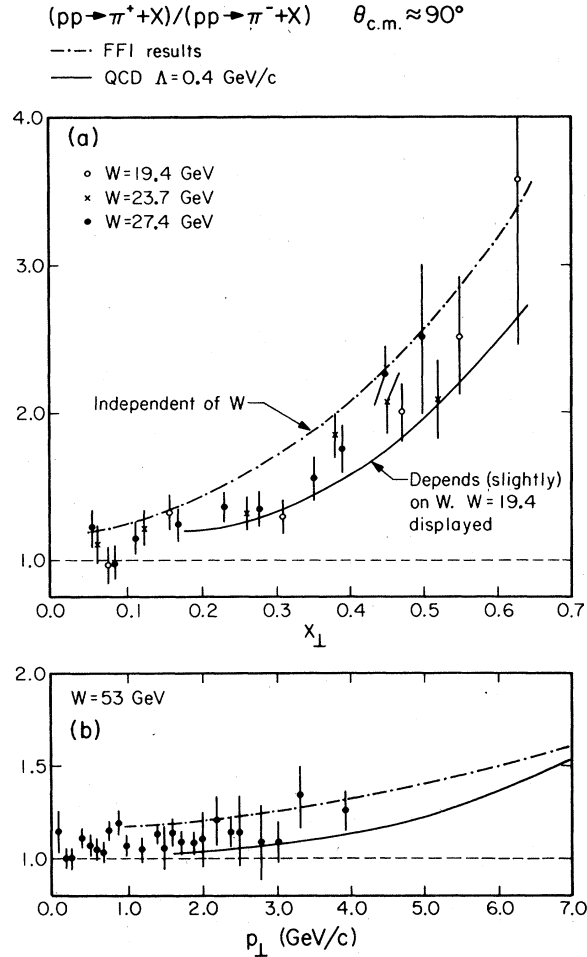
$(pp \rightarrow \pi^+ + X)/(pp \rightarrow \pi^- + X)$ $\theta_{c.m.} \approx 90°$

—·— FFI results

—— QCD $\Lambda = 0.4$ GeV/c

FIG. 13. (a) Comparison of the data (Refs. 73 and 80), of the π^+/π^- ratio in pp collisions at $\theta_{c.m.} = 90°$ versus $x_\perp$ with the quark-quark scattering model of FF1 (which is independent of W at fixed $x_\perp$) and the QCD results using $\Lambda = 0.4$ GeV/c. The QCD results are plotted for $W = 19.4$ GeV and are not precisely independent of W. The π^+/π^- ratio increases at fixed $x_\perp$ and $\theta_{c.m.}$ as W increases (by about 20% in going from 19.4 to 53 GeV). (b) Comparison of the data (Ref. 74) at $W = 53$ GeV on $pp \rightarrow (\pi^+/\pi^-) + X$ at $\theta_{c.m.} = 90°$ versus $p_\perp$ with the QCD results.

smaller than in the quark-quark scattering approach. Figures 16, 17, and 18 show that the number of away hadrons carrying a certain fraction z_p of the trigger momentum is predicted to be 3 to 4 times less than the FFF results, and now agrees quite well with experiment. This reduction in the away-side multiplicity function, $n(z_p)$ is due to three factors. First, we have increased $\langle k_\perp \rangle_{h \rightarrow q}$ from 500 to 848 MeV. This results in the large Q_x values shown in Table I (compare with Table V in FFF) and thus to a reduction of $n(z_p)$. Second, the fragmentation functions $D_q^h(z, Q^2)$ de-
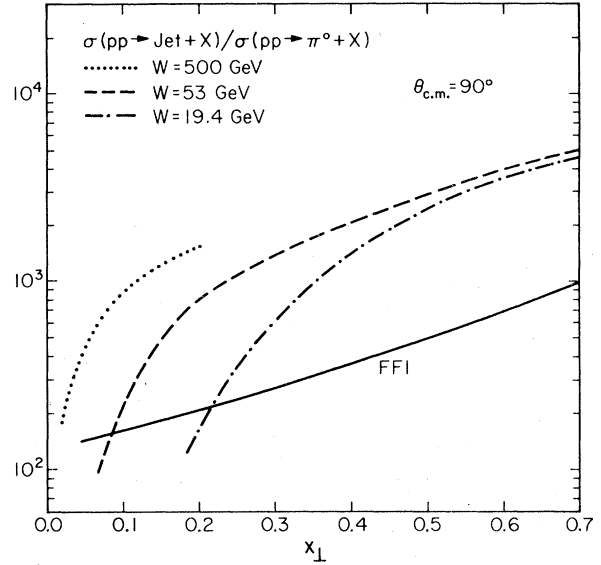
FIG. 14. Prediction of the jet-to-single-π^0 ratio $\theta_{c.m.}$ $= 90°$ versus $x_\perp$ for $W = 500$, 53, and 19.4 GeV from the QCD approach using $\Lambda = 0.4$ GeV/c. The jet cross section is defined as the cross section for producing a parton (quark + antiquark + gluon) with the given $x_\perp$. Also shown is the prediction from the quark scattering model of FF1 which is independent of W at fixed $x_\perp$ and $\theta_{c.m.}$.
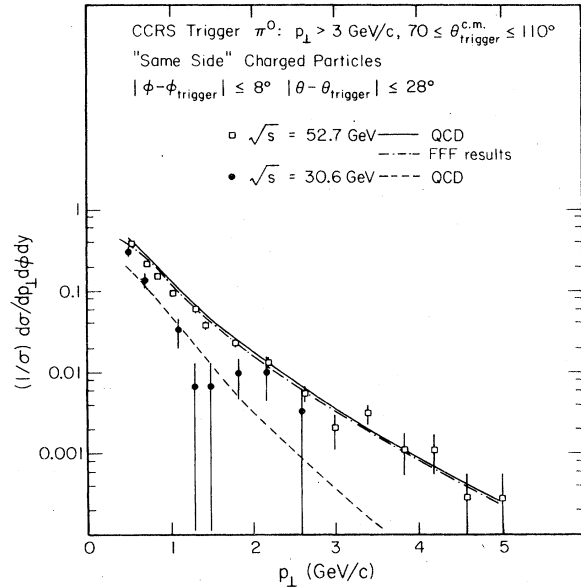

FIG. 15. Toward-side correlation measurements from CCRS collaboration (Ref. 75) together with the predictions of the QCD approach with $\Lambda = 0.4$ GeV/c and the results of the quark-quark black-box model of FFF. Possible background contributions from the fragmentation of the beam and target are *not* included.
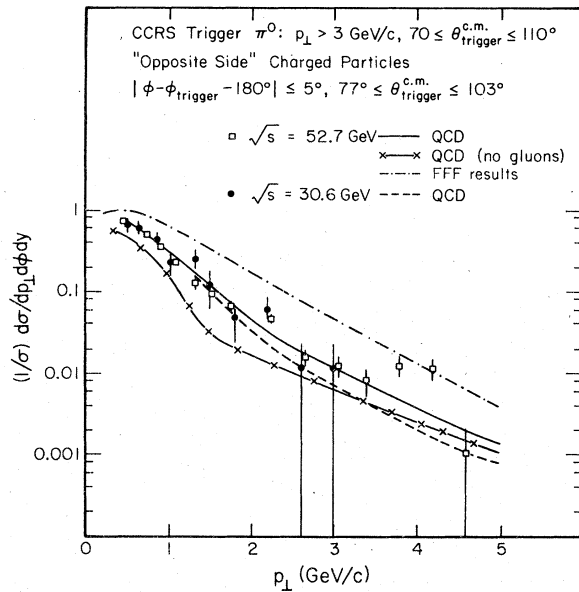
FIG. 16. Opposite or away-side correlation measurements from the CCRS collaboration (Ref. 75) together with the prediction of the QCD approach with $\Lambda = 0.4$ GeV/c and the results of the quark-quark black-box model of FFF. Possible background contribution from the beam and target jets have *not* been included.
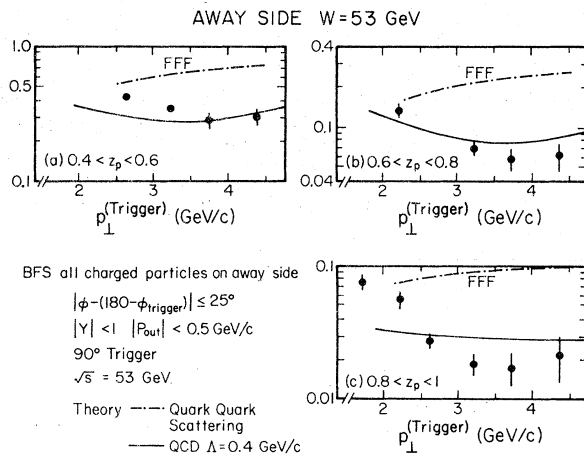

FIG. 17. The dependence on the trigger $p_\perp$ of the away-side hadron multiplicity $n(z_p) = (1/\sigma)d\sigma/dz_p$, where z_p $= -p_x$ (away)/$p_\perp$ (trig) from the British-French-Scandinavian collaboration (Ref. 43) on $pp \to h_1^\pm + h_2^\pm + X$ at W $= 53$ GeV, $\theta_1 = 90°$ and with an away-side acceptance of $25°$ in ϕ and $|Y_2| < 1$, $|P_{out}| < 0.5$ GeV/c. The predictions from the QCD approach with $\Lambda = 0.4$ GeV/c (solid curves) and the results of the quark-quark black-box model of FFF (dash-dot curves) are shown. Background contributions from the fragmentation of the beam and target (see Fig. 1 and Fig. 6) which might be important for low-$p_\perp$ triggers have *not* been included in either the QCD or FFF predictions.
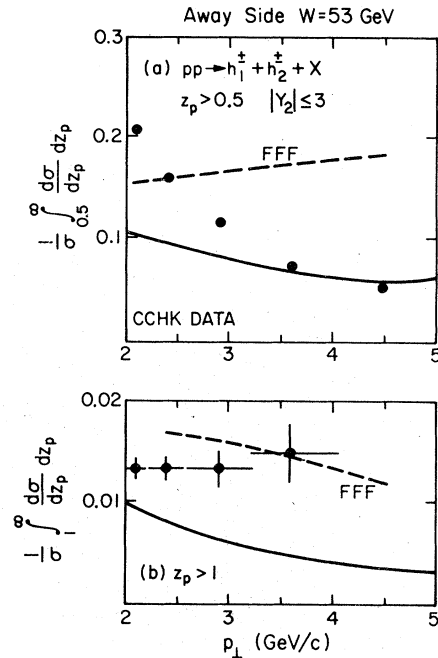
FIG. 18. The dependence on the trigger $p_\perp$ of the number of away-side hadrons per trigger with $z_p \geq 0.5$ (a) and $z_p \geq 1.0$ (b) from the CCHK collaboration (Ref. 15) on pp $\to h_1^\pm + h_2^\pm + X$ at $W = 53$ GeV, and θ_1 averaged over $45°$ and $20°$ with an away-side acceptance of $40°$ in ϕ and $|Y_2|$ ≤ 3. The predictions from the QCD approach with $\Lambda = 0.4$ GeV/c (solid curves) and the results from the quark-quark black-box model of FFF (dashed curves) are shown. Background contributions from the beam and target jets (see Fig. 1 and Fig. 6) which might be important for low-$p_\perp$ triggers have *not* been included in either the QCD or FFF predictions.

crease as Q^2 increases (see Fig. 5) and are smaller at high z than the FFF values (which now correspond to $Q^2 = Q_0^2 = 4$ GeV^2). Finally, in the QCD approach, the away-side constituent is quite often a gluon (see Tables III and IV) which produces on the average fewer hadrons at large z_p than do quarks (see Fig. 19). However, as Table V and Fig. 16 show, the number of away hadrons with $z_p \geq 0.5$ arising from gluon jets is still about half the total. (The fraction decreases as $x_\perp$ increases.) This means that the away-side multiplicity $n(z_p)$ is sensitive to the essentially unknown gluon distributions $G_{p \to g}(x, Q^2)$ and $D_g^h(z, Q^2)$.

For both the QCD approach and the quark scattering model, the away-side multiplicity function, $n(z_p)$, is roughly independent of the trigger momentum over the range $2.0 \lesssim p_\perp(\text{trig}) \lesssim 6.0$ GeV/c at $W = 53$ GeV. This means that the rise in the data (Figs. 17 and 18) at small $p_\perp(\text{trig})$ must be ascribed to "background" from the beam and target jets (see Fig. 1). We do not know how to cal-

Away Side
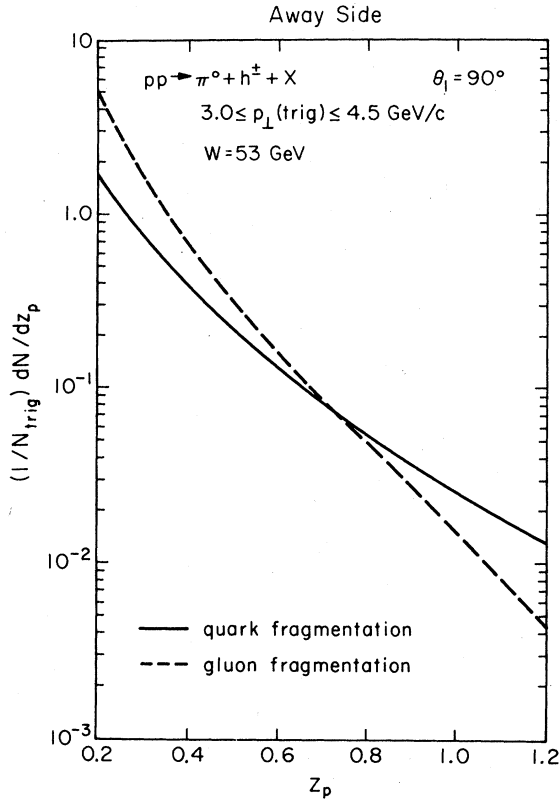

FIG. 19. The number of away-side charged hadrons per trigger, $n(z_p)$, arising from the case that the away-side constituent is a quark or antiquark (solid curve) or a gluon (dashed curve) from the QCD approach with Λ = 0.4 GeV/c. The results are calculated for $pp \to \pi^0 + h^\pm + X$ at W = 53 GeV, $\theta_1 = 90°$ with 3.0 $\leq p_\perp$ (trig) ≤ 4.5 GeV/c.

culate this properly at present, but estimates we have made indicate that this is indeed possible.[60] The rise at small $p_\perp$(trig) in the CCHK experiment (Fig. 18) is larger than that seen in experiment R-413 (Fig. 17) because the former has an away-side rapidity cut of $|Y| \leq 3$ while the latter has $|Y| \leq 1$. The CCHK experiment thus receives

a larger background contamination at low $p_\perp$(trig) particularly from the Type I background shown in Fig. 6.

2. Away-side particle ratios

Another effect of the presence of gluons is that the away-side positive to negative particle ratios at the ISR (low $x_\perp$) are predicted to be considerably different than in FFF. Figure 20 shows that the QCD approach yields almost equal numbers of positives and negatives for $p_\perp$(away) > 1.5 GeV/c at W = 53 GeV and 3.0 $\leq p_\perp$(trig) ≤ 4.0 GeV/c in agreement with the recent ISR data.[43] If the away-side constituent is always a quark or antiquark as in FFF, then this ratio is predicted to be about 1.5 in gross disagreement with the experiment.[38] However, both the FFF model and the QCD approach predict little dependence of the away-side particle ratios on the type of trigger species (i.e., π^+, π^-, K^+, K^-). This is because the scattering forces do not involve flavor exchange (they are due to gluon exchange). Neither the QCD approach nor the FFF model can explain the apparently large increase in the away-side positive to negative ratio when triggering on K^- observed by R-413 (Fig. 20). The discrepancy can be seen more clearly in Fig. 21 where we compare the predictions for the away-side rapidity spectrum of positives and negatives for a π^- and K^- trigger with the preliminary R-413 data.[43]

This question of the flavor dependence of the constituent subprocesses is an important one. In models such as the constituent-interchange model (CIM),[56,61] the scattering forces arise from the exchange of quarks which carry flavor.[62] In these models, drastic changes can occur in the away-side particle ratios as one changes trigger species.[63] Figure 22 shows data from the Fermilab experiment E-494 (Ref. 64) on the away-side multiplicity of π^+, π^-, K^+, and K^- with $z_p \geq 0.5$ for a trigger meson of type π^+, π^-, K^+, K^- at W

TABLE V. Total away-side multiplicity (Ref. 59), $N(z_p \geq 0.5)$, per trigger for charged hadrons in the processes $pp \to \pi^0 + h^\pm + X$ at $\theta_1 = 90°$ predicted from the QCD approach with $\Lambda = 0.4$ GeV/c. Also shown are the individual contributions to the multiplicity for $z_p \geq 0.5$ from gluon and quark fragmentation. [The function $N(z_p^0, P_{\perp 1}, \theta_1)$ is defined by Eqs. (6.1) and (6.2) in FFF.]

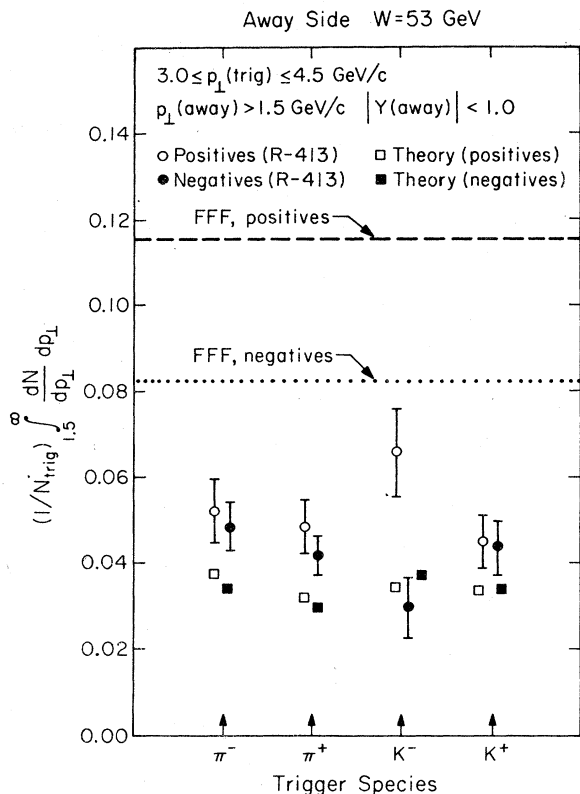| W (GeV)	$P_\perp$ (GeV/c)	$x_\perp$	Quark fragmentation	Gluon fragmentation	Total $z_p \geq 0.5$
53	2.0	0.08	0.047	0.083	0.130
53	3.4	0.13	0.052	0.050	0.102
53	4.5	0.17	0.058	0.047	0.105
53	5.3	0.20	0.063	0.038	0.101
53	9.3	0.35	0.060	0.022	0.082
53	13.2	0.50	0.058	0.014	0.072

FIG. 20. The number of away-side positive and nega-tive hadrons with $p_\perp$ (away) > 1.5 GeV/c per trigger with $3.0 \leq p_\perp$ (trig) ≤ 4.5 GeV/c from the BFS collaboration (R-413) (Ref. 43) on $pp \to h_1 + h^\pm + X$ where $W = 53$ GeV and $\theta_1 = 90°$ and $|Y_2| < 1.0$. The results for π^-, π^+, K^-, and K^+ triggers are shown and compared to the predic-tions of the quark-quark black-box model of FFF and the QCD approach with $\Lambda = 0.4$ GeV/c (open and solid squares). Background contributions from the beam and target jets (see Figs. 1 and 6) have *not* been included in either the QCD or FFF predictions.

FIG. 21. The away-side rapidity distributions, $(1/N_{\text{trig}})$ dN/dY, of positive and negative hadrons with $p_\perp$ (away) > 1.5 GeV/c for 90° π^- and K^- triggers in the range 3.0 $\leq p_\perp$ (trig) ≤ 4.5 GeV/c from the BFS collaboration (R-413) (Ref. 43). Predictions of the QCD approach with Λ $= 0.4$ GeV/c are shown where background contributions from the beam and target jets (see Figs. 1 and 6) have not been included.

$= 27.4$ GeV and $3.0 \leq p_\perp$(trig) ≤ 5.0 GeV/c compared to the QCD predictions. The agreement is quite good. The away-side ratios are roughly indepen-dent of the trigger species and given approximately by the single-particle ratios (shown by the wiggly arrows along the side) which is just as expected for a flavorless-exchange constituent subprocess. There is a slight disagreement for the K^- trigger but the data *do not* show the large positive plus negative sum seen by R-413. In fact, the away-side number of K^+ mesons with a K^- trigger is correctly predicted. The data in Fig. 22 from E-494 are taken off a beryllium target and there are A-dependence corrections[64] (we have made no A-dependence correction to our theoretical pre-dictions) that make direct comparison a bit dangerous. Because of this and because of the apparent disagreement between R-413 and E-494
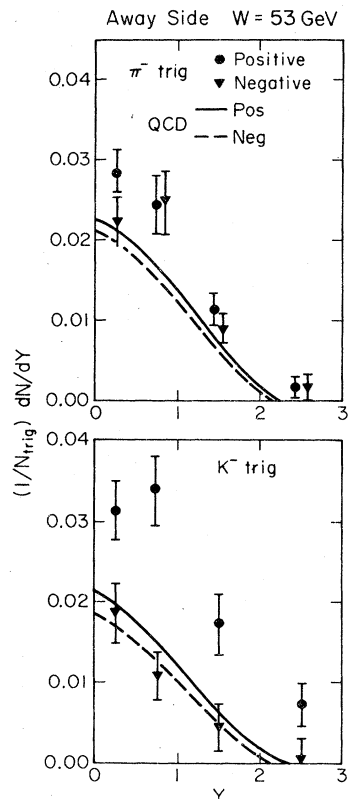
for K^- triggers the question as to whether or not there is any evidence for flavor exchange in the constituent subprocess is unsettled.

3. P_{out}

Due to our use of $\langle k_\perp \rangle_{h \to q} = 848$ MeV and $\langle k_\perp \rangle_{q \to h}$ $= 439$ MeV, the mean values of P_{out} are predicted to be considerably larger than the results of FFF ($\langle k_\perp \rangle_{h \to q} = 500$ MeV, $\langle k_\perp \rangle_{q \to h} = 330$ MeV). In Figs. 23 and 24, we compare both the new QCD results and the FFF results with the mean values of P_{out} obtained in the CCHK experiment.[15] The value of $\langle k_\perp \rangle_{h \to q} = 848$ MeV, obtained from the fit to the data on $pp \to \mu^+ \mu^- + X$ shown in Fig. 7, results in $\langle P_{\text{out}} \rangle$ values that agree better with the hadron experi-ments, although they are still a bit small. (Some of the discrepancies may be due to contributions from the beam and target jets omitted in our analysis.)
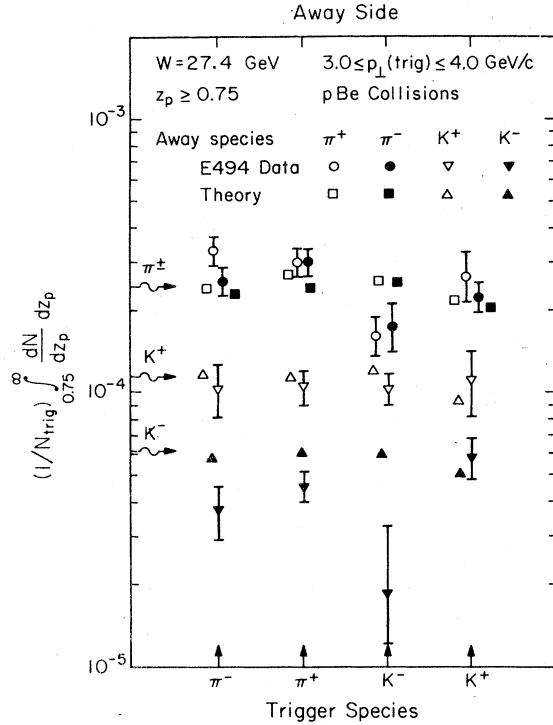
FIG. 22. The number of away-side mesons (of type π^+, π^-, K^+, K^-) with $z_p \geq 0.75$ per trigger (of type π^+, π^-, K^+, K^-) from the Fermilab experiment E494 (Ref. 64). The data are taken at $W = 27.4$ GeV with $3.0 \leq p_\perp$(trig) ≤ 4.0 for proton-beryllium collisions and are compared with the prediction of the QCD approach (for proton-proton collisions) with $\Lambda = 0.4$ GeV/c. No A-dependence corrections have been made to the theory or the data.

4. Experimental tests for effects due to $\langle k_\perp \rangle_{h \to q}$

As seen in Figs. 2 and 8, the basic constituent subprocess of QCD (before smearing) behaves roughly like $1/p_\perp^6$ at fixed $x_\perp$ for $2 \leq p_\perp \leq 10$ GeV/c. The experimentally observed $1/p_\perp^8$ behavior is obtained by including the effects of smearing ($\langle k_\perp \rangle_{h \to q} \neq 0$) which raise the small-$p_\perp$ prediction while leaving the large-$p_\perp$ region essentially unchanged. This increase at small $p_\perp$, due to the "trigger bias" effect, can be partially removed by triggering on events with equally large $p_\perp$'s on the toward and away-side (i.e., $z_p \approx 1$).[65,66] Thus, in general, we expect the $p_\perp$ dependence of the two-particle back-to-back cross section to differ (in the region where smearing is an important effect) from that of the single-particle cross section. This is seen in Fig. 25 where we plot the two-particle back-to-back cross section $d\sigma/dz_p$ at $z_p = 1$ (times $p_\perp^8$) versus $p_\perp$ at $x_\perp = 0.35$. It behaves roughly like $1/p_\perp^6$ over the range $4 \leq p_\perp \leq 6.0$ GeV/c whereas the single-particle cross-section results, when multiplied by $p_\perp^8$,
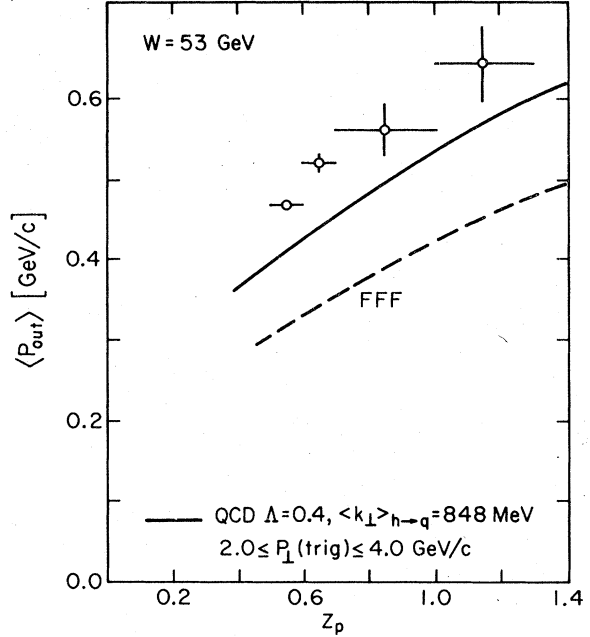

FIG. 23. The dependence on z_p of the mean value of the $|P_{out}|$ of away-side charged hadrons at $W = 53$ GeV and $2.0 \leq p_\perp$(trig) ≤ 4.0 GeV/c with θ_1 averaged over 45° and 20° from the CCHK collaboration (Ref. 15) on $pp \to h_1^\pm + h_2^\pm + X$. The predictions from the QCD approach at $\theta_1 = 45°$ with $\Lambda = 0.4$ GeV/c and $\langle k_\perp \rangle_{h \to q} = 848$ MeV (solid curve) and the results of FFF (dashed curve) curve are shown.
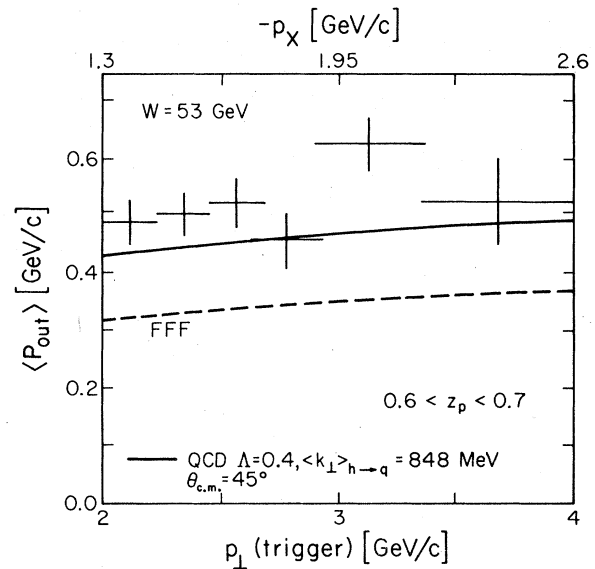

FIG. 24. The dependence on the trigger $p_\perp$ of the mean value of the $|P_{out}|$ of away-side charged hadrons with $0.6 \leq z_p \leq 0.7$ at $W = 53$ GeV and θ_1 averaged over 45° and 20° from the CCHK collaboration (Ref. 15) on $pp \to h_1^\pm + h_2^\pm = X$. The predictions for $\theta_1 = 45°$ from the QCD approach with $\Lambda = 0.4$ GeV/c and $\langle k_\perp \rangle_{h \to q} = 848$ MeV, $\langle k_\perp \rangle_{q \to h} = 439$ MeV (solid curve) and the FFF results (dashed curve) are shown.
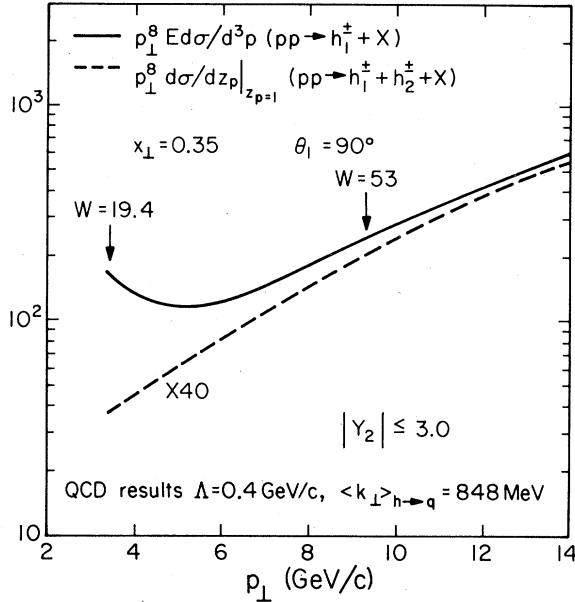
FIG. 25. Comparison of the behavior of $p_\perp^8$ times the single-charged-particle cross section $Ed\sigma/d^3p$ $(pp \to h_1^\pm + X)$, and $p_\perp^8$ times the two-particle back-to-back cross section $d\sigma/dz_p|_{z_p=1}$ $(pp \to h_1^\pm + h_2^\pm + X)$ at *fixed* $x_\perp = 0.35$ (times 40). The QCD predictions are calculated at θ_1 $= 90°$ with $\Lambda = 0.4$ GeV/c and $\langle k_\perp \rangle_{h \to q} = 848$ MeV.

are roughly independent of $p_\perp$ over the range. The two-particle back-to-back cross section $d\sigma/ dz_p(z_p \approx 1)$ reflects more closely the dependence on $p_\perp$ of the basic subprocess without the additional scale breaking due to smearing.

The predictions in Fig. 25 (and in all figures in this paper) are free from any beam and target jet background of the type discussed in Sec. IV D 1 above. As seen in Fig. 18, below $p_\perp = 3.5$ GeV/c this background is important and is presumably the cause of the rise of dN/dz_p at low $p_\perp(\text{trig})$. Any such increase of the expected dN/dz_p at low $p_\perp$ due to background would vitiate the comparison in Fig. 25 by making it behave similarly to the single-particle cross section. The test must be performed at $p_\perp$'s large enough so that the background contamination is negligible. This is why we calculated the results in Fig. 25 at $x_\perp = 0.35$ so that $p_\perp \gtrsim 4$ GeV/c.

E. Very-high-energy expectations

Figure 8 shows that the QCD predictions quickly deviate from a $1/p_\perp^8$ behavior (at fixed $x_\perp$) as the $p_\perp$ increases yielding a much larger cross section than expected from the black-box model. This is also seen in Fig. 26 where we plot the QCD predictions for $p_\perp^8$ times $Ed\sigma/d^3p$ versus $p_\perp$ at $x_\perp$ $= 0.05$ and $\theta_{c.m.} = 90°$. At $W = 500$ GeV, the QCD
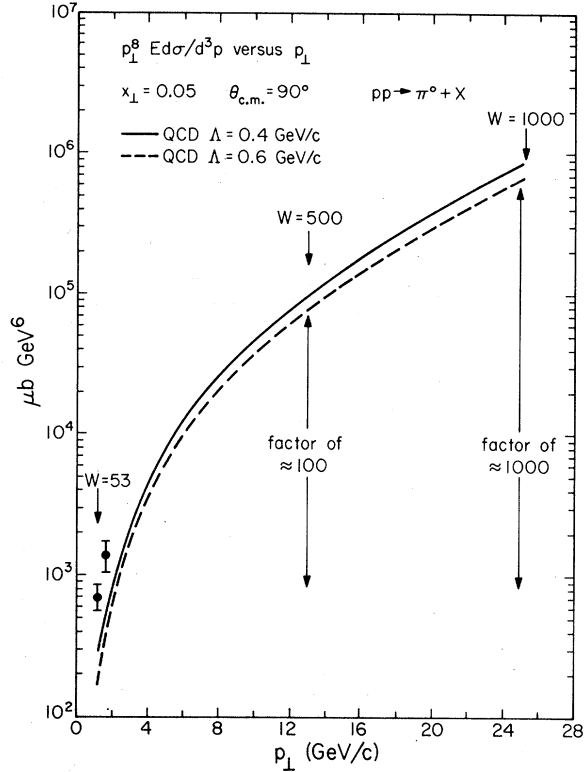

FIG. 26. The behavior of $p_\perp^8$ times the 90° single-π^0 cross section, $Ed\sigma/d^3p$, at $x_\perp = 0.05$ versus $p_\perp$ calculated from the QCD approach with $\Lambda = 0.4$ GeV/c (solid curve) and $\Lambda = 0.6$ GeV/c (dashed curve). The two low-$p_\perp$ data points are at $W = 53$ and 63 (Ref. 74). The predictions are a factor of 100 (1000) times larger than the flat $(p_\perp^{-8})$ extrapolation to $W = 500$ GeV (1000 GeV).

results are a factor of 100 larger than a straight $(1/p_\perp^8)$ extrapolation and show a factor of 1000 increase at $W = 1000$ GeV. In Fig. 27 we display the predictions for 90° π^0 and jet production at fixed $W = 53$, 500, and 1000 GeV versus $p_\perp$. The preliminary high-$p_\perp$ data from CCOR (Ref. 67) at $W = 53$ GeV are also shown. The black-box model and the QCD predictions agree with each other and both agree with the data. By going to higher energy, one can easily discriminate between the two approaches. For example, at W $= 500$ GeV and $p_\perp = 30$ GeV/c, the π^0 (jet) cross section from QCD is roughly a factor of 100 (500) times larger than the FF1 results. In fact, the $p_\perp = 30$ GeV/c 90° π^0 cross section at $W = 500$ GeV is predicted in the QCD approach to be about the same magnitude as that measured at $p_\perp = 6.0$ GeV/c at Fermilab ($W = 19.4$ GeV).

These large single-particle and jet cross sections (see also Fig. 14) predicted by QCD, if correct, will make it very difficult, if not impossible, to find the W boson (and other new parti-
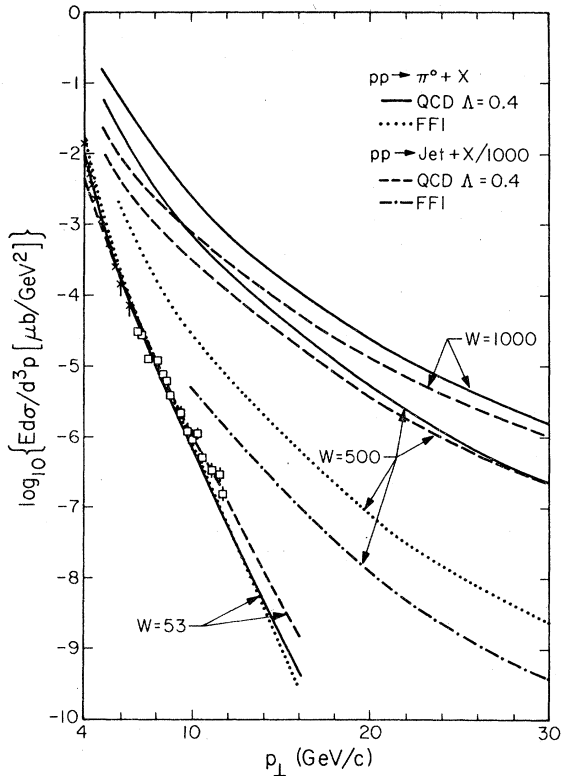
FIG. 27. Comparison of the results on the 90° π^0 cross section, $Ed\sigma/d^3p$, from the QCD approach with $\Lambda = 0.4$ GeV/c (solid curve) and the quark-quark black-box model of FF1 (dotted curves). Both models agree with the data at $W = 53$ GeV (crosses = Ref. 52) where the open squares are the "preliminary" data from the CCOR collaboration (Ref. 67) normalized to agree with the lower-$p_\perp$ experiments. The QCD approach results in much larger cross sections than the FF1 model at $W = 500$ and 1000 GeV. The FF1 results at 1000 GeV (not shown) are only slightly larger than the results at 500 GeV. Also shown are the cross sections for producing a jet at 90° (divided by 1000) as predicted by the QCD approach (dashed curves) and the FF1 model (dot-dashed curve).

cles) from its $q\bar{q}$ or jet-jet decay. Quigg[68] showed that even the black-box $(1/p_\perp^8)$ model extrapolation led to a W signal that was, at best, 10 times the hadronic (jet-jet) background. The factor of 500 (1000) increase in this background at $W = 500$ (1000) GeV predicted is obviously fatal. However, if one indeed observes such large production rate for single particles and jets, then QCD will be verified and this may be as important as discovering the W boson.

It is not clear yet precisely what the quark and gluon jets will look like at very high $p_\perp$ (such as $p_\perp = 30$ GeV/c). If QCD is correct, they will certainly not look like the well collimated $\langle k_\perp \rangle_{q \to h}$ $= 430$ MeV objects we use in this calculation and illustrated in Fig. 1. At $p_\perp = 30$ GeV/c, they should

"appear" to be fatter. This is because as the $p_\perp$ of the outgoing quark is increased, it becomes increasingly more likely that it radiate a gluon and become two jets (one quark and one gluon). Then, this quark or gluon might radiate producing still more jets. The net result is that most of the time it will look as if there is one fat jet; however, occasionally when the radiation is hard enough, one will see the two or three distinct subjets.[69-71] Much theoretical effort is being focused on such questions and we should soon have a good idea of precisely what to expect at very high energies and $p_\perp$'s.

V. SUMMARY AND CONCLUSIONS

If this work is viewed as simply a comparison of one phenomenological model against another (e.g., the QCD approach versus the black-box model), not much can be said to favor one over another. It is true that the QCD approach has fewer free parameters in the parton cross sections $d\hat{\sigma}/d\hat{t}$, but there are more free choices in the gluon functions. More excuses are needed concerning background effects at low $p_\perp$, etc. It is true that the black-box pure quark scheme could not fit the away-side large-$p_\perp$ particle multiplicities and charge ratios, but it probably could be fixed up with the inclusion of gluons. It has become apparent that present high energies are not really high enough to isolate the manifold of effects (parton distributions, fragmentation functions, constituent cross sections, transverse momentum of partons, different kinds of constituents, etc.) that are mixed together so intimately in today's experiments. If the resolution of this would depend entirely on experiment, we shall have to end this long research with the tiresome and obvious call for still higher energies. At high $p_\perp$, predictions of the QCD approach are orders of magnitude greater than the black-box $p_\perp^{-8}$ extrapolations, so clear tests lie there.

But QCD is more than a phenomenological model. It is a precise and complete theory purporting to be an ultimate explanation of all hadronic experiments of all energies, high and low. There are many reasons to hope and expect it to be right. The question is, is it indeed right? Mathematical complexity has, so far, prevented us from quantitatively testing its correctness. What it predicts is not clearly known. Nevertheless, its property of asymptotic freedom leads us to expect that phenomena of high momentum transfer should be analyzable (by perturbation theory). Yet experiments at what was thought to be high enough $p_\perp$ seemed to show $p_\perp^{-8}$ behavior unlike the expected $p_\perp^{-4}$ (with possible logarithmetic modifications).

It was a mystery. Although many people said "perhaps the energy is not high enough," the remark was simply an article of faith; the mechanism leading to an apparent eighth power in the experimental region remained unknown.

We believe we have resolved this mystery, using the QCD theory itself to tell us what might happen in the range in question. There is, from the point of view of QCD, no mystery. The energy $(p_\perp)$ is indeed too low and there are too many nonasymptotic effects acting. Results closer to a $p_\perp^{-4}$ fall-off should appear only at much higher $p_\perp$ (see Fig. 9). Machines currently planned for these energies will resolve the question of models as soon as they are turned on.

On the other side, there is a great deal of data now available at energies and $p_\perp$ values in which asymptotic free field theory can make much more precise predictions than have yet been made. The QCD theory, unlike other phenomenological approaches, is complete mathematically so that a full discussion of theoretical predictions with limits of errors should be possible in the present range. These theoretical studies (perhaps starting at very high energy and working down) should be pursued vigorously. It is likely that among the present results of experiment, there are some that can contribute a more precise and definite test of QCD, if the theory could be developed a little further and made a bit more precise than we have done here. At the time of this writing, there is still no sharp quantitative test of QCD. An important test will come in connection with the phenomena of high $p_\perp$ discussed here.

ACKNOWLEDGMENTS

[1]R. D. Field and R. P. Feynman, Phys. Rev. D 15, 2590 (1977).

[2]R. P. Feynman, R. D. Field, and G. C. Fox, Nucl. Phys. B128, 1 (1977).

[3]R. Baier, J. Cleymans, K. Kinoshita and B. Peterson, Nucl. Phys. B118, (1977).

[4]E. Fischbach and G. W. Look, Phys. Rev. D 15, 2576 (1977); G. W. Look and E. Fischbach, ibid. 16, 1369 (1977).

[5]W. Furmanski and J. Wosiek, Acta Phys. Pol. B8, 633 (1977); B8, 649 (1977).

[6]J. Kripfganz and J. Ranft, Nucl. Phys. B124, 351 (1977); E. M. Ilgenfritz, J. Kripfganz, H. J. Mohring, G. Ranft, J. Ranft, and A. Schiller, Acta. Phys. Pol. B9, 15 (1978); A. Schiller, E. M. Ilgenfritz, J. Kripfganz, H. J. Mohring, G. Ranft and J. Ranft, ibid. B9, 31 (1978).

[7]M. K. Chase and W. J. Stirling, Nucl. Phys. B133, 157 (1978).

[8]D. Duke, Phys. Rev. D 16, 1375 (1977).

[9]A. P. Contogouris and R. Gaskell, Nucl. Phys. B126, 157 (1977).

[10]P. V. Landshoff, talk presented at the Workshop on Future ISR Physics, 1977, edited by M. Jacob (unpublished).

[11]M. Fontannaz and D. Schiff, Nucl. Phys. B132, 457 (1978).

[12]M. K. Chase, University of Cambridge Report No. DAMTP 77/29, 1977 (unpublished).

[13]R. Raitio and R. Sosnowski, University of Helsinki Report No HU-TFT-77-22, invited talk given at the Workshop on Large $p_\perp$ Phenomena, University of Bielefeld, 1977 (unpublished).

[14]R. Baier and B. Petersson, University of Bielefeld Report No. BI-TP77/08 (unpublished).

[15]M. Della Negra et al. (CCHK Collaboration), Nucl. Phys. B127, 1 (1977).

[16]Effects due to the transverse momentum of the partons in the initial hadrons have been seen directly in the recent Fermilab jet-jet experiment of L. Cormell et al.,

Fermilab Report No. 77-89, 1977 (unpublished).

[17]H. Georgi and H. D. Politzer, Phys. Rev. D 14, 1829 (1976).

[18]G. C. Fox, Nucl. Phys. B131, 107 (1977).

[19]A. J. Buras, E. G. Floratos, D. A. Ross, and G. T. Sachrajda, Nucl. Phys. B131, 308 (1977); A. J. Buras and K. J. F. Gaemers, ibid. 132, 249 (1978).

[20]H. L. Anderson, H. S. Matis, and L. C. Myrianthopoulos, Phys. Rev. Lett. 40, 1061 (1978); H. Anderson and T. Quirk, private communication.

[21]R. D. Field, Phys. Rev. Lett. 40, 997 (1978).

[22]G. C. Fox, invited talk presented at the Orbis Scientiae, Coral Gables, 1978 (unpublished).

[23]See also Refs. 13, 24, and 25.

[24]A. P. Contogouris, R. Gaskell, and A. Nicolaidis, McGill University report, 1977 (unpublished); A. P. Contogouris, R. Gaskell, and S. Papadopoulos, McGill University report 1978 (unpublished).

[25]S. D. Ellis, in Particles and Fields—1977, Proceedings of the Meeting of the APS Division of Particles and Fields, edited by P. A. Schreiner, G. H. Thomas, and A. B. Wickland (AIP, New York, 1978).

[26]H. D. Politzer, Phys. Rep. 14C, 129 (1974); invited talk at the Ben Lee Memorial Conference, 1977 [Report No. CALT-68-628 (unpublished)].

[27]R. D. Field and R. P. Feynman, Nucl. Phys. B136, 1 (1978).

[28]R. Cutler and D. Sivers, Phys. Rev. D 16, 679 (1977); 17, 196 (1978).

[29]B. L. Combridge, J. Kripfganz, and J. Ranft, Phys. Lett. 70B, 234 (1977).

[30]G. Altarelli, G. Parisi, and R. Petronzio, Phys. Lett. 76B, ibid. 351 (1978); G. Altarelli, G. Parisi, and R. Petronzio, 76B, 356 (1978).

[31]K. H, Craig and C. H. Llewellyn Smith, Phys. Lett. 72B, 349 (1978).

[32]H. Fritzsch and P. Minkowski, Phys. Lett. 73B, 180 (1978).

[33]K. Kajantie and R. Raitio, Nucl. Phys. B139, 72 (1978).

[34]J. F. Martin et al., Phys. Rev. Lett. 40, 283 (1978).

[35]G. Donaldson et al., Phys. Rev. Lett. 40, 917 (1978).

[36]C. Bromberg et al., invited talk by E. Malamud at the VII International Symposium on Multiparticle Dynamics, Kayersberg, France, 1977 (unpublished).

[37]M. D. Corcoran et al., Phys. Rev. Lett. 41, 9 (1978).

[38]See also G. C. Fox, in Particles and Fields -1977, proceedings of the Meeting of the Division of Particles and Fields of the APS, edited by P. A. Schreiner, G. H. Thomas, and A. B. Wicklund (AIP, New York, 1978).

[39]See also S. D. Ellis, M. Jacob, and P. V. Landshoff, Nucl. Phys. B108, 93 (1976); M. Jacob and P. Landshoff, ibid. B113, 395 (1976).

[40]C. Bromberg et al., Nucl. Phys. B134, 189 (1978); C. Bromberg et al., Phys. Rev. Lett. 38, 1447 (1977).

[41]G. C. Fox, in Particles and Fields '76, proceedings of the Annual Meeting of the Division of Particles and Fields of the APS, edited by H. Gordon and R. F. Peierls (BNL, Upton, New York, 1977), p.G1.

[42]We use the same notation as defined in Table I and Fig. 2 of FFF. The fractional momenta z_p is given by $z_p = -p_x (h_2)/p_\perp(h_1)$, where h_1 and h_2 are the trigger and away-side hadron, respectively, and p_x is the perpendicular component of momentum in the scattering plane formed by the trigger, beam, and target.

[43]H. Boggild (British-French-Scandinavian Collaboration), invited talk at the Eighth Symposium on Multiparticle Dynamics, Kayersberg, France 1977 (unpublished); R. Moller, in Leptons and Multileptons, proceedings of the XII Recontre de Moriond, edited by J. Tran Thanh Van (Editions Frontieres, Paris, 1977).

[44]In addition to the $\ln(Q^2/\Lambda^2)$ variation in the denominator of Eq. (3.1), there is, in a more precise analysis, a term of the form $\ln [\ln(Q^2/\Lambda^2)]$ whose variation with Q^2 we have neglected. See W. E. Caswell, Phys. Rev. Lett. 33, 244 (1974).

[45]W. B. Atwood et al., Phys. Lett. 64B, 479 (1976); W. B. Atwood, SLAC Report No. SLAC-185, thesis, 1975 (unpublished).

[46]Although in this paper we have calculated with the old solutions of Ref. 18, we have verified that the new data lead only to small changes in these solutions. In particular, the best value of Λ is unchanged.

[47]J. F. Owens, Phys. Lett. 76B, 85 (1978).

[48]The matrix $\bar{R}_{ij}$ is simply the transpose of R_{ij}.

[49]D. J. Gross, Phys. Rev. Lett. 32, 1071 (1974).

[50]M. G. Albrow et al., Nucl. Phys. B135, 461 (1978).

[51]D. C. Hom et al., Phys. Rev. Lett. 36, 1239 (1976), 37, 1374 (1976); S. W. Herb et al., ibid. 39, 252 (1977); W. R. Innes et al., ibid. 39, 1240 (1977).

[52]See also J. F. Owens, E. Reya, and M. Gluck, Phys. Rev. D 18, 1501 (1978).

[53]See also F. Halzen, G. A. Ringland, and R. G. Roberts, Phys. Rev. Lett. 40, 991 (1978).

[54]To avoid divergences due to increasing $\alpha_s(Q^2)$ at low Q^2 in (3.1), we never allow Q^2 to be smaller than our reference momentum $Q_0^2 = 4$ GeV^2 [i.e., Q^2 is given by (3.2) if it is greater than Q_0^2 and set equal to Q_0^2 elsewhere].

[55]At $W = 19.4$ GeV, $\theta = 90°$ and $p_\perp = 1.94$ GeV/c changing the cutoff M_0^2 from 1.0 GeV^2 to 0.3 GeV^2 causes a factor of 2 increase in the resulting invariant cross section for $pp \to \pi^0 + X$. Increasing M_0^2 to 3.0 GeV^2 decreases the cross section at this energy and $p_\perp$ by about a factor of 2.

[56]R. Blankenbecler, S. J. Brodsky, and J. F. Gunion, Phys. Rev. D 18, 900 (1978).

[57]R. D. Field, in Leptons and Multileptons, proceedings of the XII Recontre de Moriond, edited by J. Tran Thanh Van (Editions Frontieres, Paris, 1977).

[58]The quantity z_c is the fraction of the toward-side parton momentum carried by the trigger hadron (see Fig. 1).

[59]The away-side multiplicity distribution, $n(z_p) \equiv [1/N$ (trig)] dN(away)$/dz_p$, is the number of away hadrons between z_p and $z_p + dz_p$ per trigger hadron, where z_p is defined in Ref. 42. See Eqs. (6.1) and (6.2) of FFF.

[60]See also the estimates made in Ref. 15.

[61]R. Blankenbecler, S. J. Brodsky, and J. F. Gunion, Phys. Rev. 106, 2652 (1972); Phys. Lett. 42B, 461 (1973); R. Blankenbecler and S. J. Brodsky, Phys. Rev. D 10, 2973 (1974); R. Blankenbecler, S. J. Brodsky, and J. Gunion, ibid. 12, 3469 (1975); R. Raitio and G. Ringland, ibid. 14, 2291 (1976).

[62]Some of the QCD terms in Table I such as $gg \to q\bar{q}$ do have a strong correlation between the toward and away quark flavor; however, these terms contribute little to the total single-particle rate and thus have only a very small effect.

[63]S. J. Brodsky, invited talk at the VIII International Symposium on Multiparticle Dynamics, Kayersberg, France, 1977 [SLAC Report No. SLAC-PUB-2009 (unpublished)].

[64]R. J. Fisk et al., Phys. Rev. Lett. 40, 984 (1978); R. J. Engelmann, private communication.

[65]B. Combridge, in ISR Discussion Meeting Between Theorists and Experimentalists Number 21, 1977, edited by M. Jacob (unpublished).

[66]Other ways of eliminating this trigger bias have been suggested by W. Ochs and L. Stodolsky, Phys. Lett. 69B, 225 (1977). Also see P. V. Landshoff and J. C. Polkinghorne, Phys. Rev. D 18, 3344 (1978).

[67]CERN-Columbia-Oxford-Rockefeller Experiment, reported by L. D. Lella in the Workshop on Future ISR Physics, 1977, edited by M. Jacob (unpublished).

[68]C. Quigg, Rev. Mod. Phys. 49, 297 (1977); also, R. F. Peierls, T. L. Trueman, and L. L. Wang, Phys. Rev. D 16, 1397 (1977).

[69]G. Sterman and S. Weinberg, Phys. Rev. Lett. 39, 1436 (1977).

[70]J. Ellis, M. K. Gaillard, and G. G. Ross, Nucl. Phys. B111, 253 (1976).

[71]A. De Rujula, J. Ellis, E. G. Floratos, and M. K. Gaillard, Nucl. Phys. B138, 387 (1978).

[72]The points at $x = 0.5$ correspond to all the SLAC data referred to in Table I of Ref. 18.

[73]J. W. Cronin et al. (CP Collaboration), Phys. Rev. D 11, 2105 (1975); D. Antreasyan et al., Phys. Rev. Lett. 38, 112 (1977); 38, 115 (1977).

[74]B. Alper et al. (BS Collaboration), Nucl. Phys. B100, 237 (1975).

[75]F. W. Busser et al., Nucl. Phys. B106, 1 (1976).

[76]G. Donaldson et al., Phys. Rev. Lett. 36, 1110 (1976).

[77]D. C. Carey et al., Fermilab Report No. FNAL-PUB-75120-EXP, 1975 (unpublished).

[78]M. B. Albrow et al. (CHLM Collaboration), Nucl. Phys. B73, 40 (1974).

[79]R. Cottrell et al., Phys. Lett. 55B, 341 (1975).

[80]H. Frisch, in Particles and Fields '76, proceedings of the Annual Meeting of the Division of Particles and Fields of the APS, edited by H. Gordon and R. F. Peierls (BNL, Upton, New York, 1977), p. F59.